DISSERTATIONES
ASTRONOMIAE
UNIVERSITATIS
TARTUENSIS
17

RAIN KIPPER

Galaxy modelling: dynamical methods and applications

DISSERTATIONES ASTRONOMIAE UNIVERSITATIS TARTUENSIS

17

DISSERTATIONES ASTRONOMIAE UNIVERSITATIS TARTUENSIS
17

RAIN KIPPER

Galaxy modelling: dynamical methods and applications

UNIVERSITY OF TARTU
Press

This study was carried out at Tartu University and Tartu Observatory, Estonia.

The Dissertation was admitted on 23.05.2016, in partial fulfilment of the requirements for the degree of Doctor of Philosophy in physics (astrophysics), and allowed for defence by the Council of the Institute of Physics, University of Tartu.

Supervisors: Dr. Elmo Tempel,
Tartu Observatory,
Estonia

Prof. Peeter Tenjes,
Institute of Physics, University of Tartu,
Estonia

Opponents: Dr. Pekka Heinämäki,
Tuorla Observatory
Finland

Dr. Gert Hütsi,
Tartu Observatory
Estonia

Defence: 31.08.2016, University of Tartu, Estonia

ISSN 1406-0302
ISBN 978-9949-77-131-8 (print)
ISBN 978-9949-77-132-5 (pdf)

University of Tartu Press
www.tyk.ee

CONTENTS

List of original publications **7**

Introduction **10**

1 Overview of dynamic modelling **12**
1.1 The importance of dynamic modelling 12
1.2 Overview of dynamic modelling 13
1.2.1 Models based on the phase density distribution 13
1.2.2 Modelling based on the Jeans equations 15
1.2.3 Models based on the Schwarzschild orbit superposition . . . 19
1.2.4 Numerical simulations of galaxy dynamics 20

2 Modelling the dynamics of a galaxy with the Jeans equations **21**
2.1 Jeans equations in a general form 21
2.2 Modelling the dynamics of a gas component in a galaxy 23
2.3 Modelling the dynamics of a stellar component 24
2.3.1 Tri-axiality of the stellar velocity dispersions 24
2.3.2 Constraining the velocity ellipsoid with a third integral of motion 26
2.3.3 The solution of the Jeans equations and its consistency with the third integral of motion 29

3 From dynamical model to measured kinematics **32**
3.1 Line of sight effects in external galaxies 32
3.1.1 Integration of functions over the line of sight 32
3.1.2 Integrating kinematic quantities over the line of sight 34
3.1.3 Integration over the line of sight in presence of dust 36
3.2 Additional kinematic effects inside external galaxies 37
3.3 Distortions of kinematics in atmosphere and instrumentation 38
3.3.1 Distortions due to seeing and slit width of a spectrograph . . 39
3.3.2 Extracting kinematics from spectroscopic data 41

4 Density distribution estimation **42**
4.1 Modelling the density profiles 42
4.1.1 The procedure of photometrical modelling 42
4.1.2 The Einasto profile 44
4.2 Reliability of the parameters of photometric model 45
4.2.1 Test-galaxies for estimating robustness of photometric model 45

4.2.2 The reliability of the photometric model parameters 46
4.3 Adding the dark matter and the gas to the overall density distribution 48

5 Applying the model to observed galaxies 51
5.1 Applying the gas dynamic model 51
5.1.1 The data and assumptions for the dynamic model 51
5.1.2 Comparison of the model gas kinematics with observations . 52
5.2 Modelling of an example galaxy – Andromeda galaxy 55
5.2.1 The data and assumptions for the dynamic model 55
5.2.2 Comparison of the model stellar kinematics with observations 59

6 Dust effects in the observed kinematics of a galaxy 65
6.1 The effect of the dust attenuation to model kinematics 65
6.2 Dependence of rotational velocities and velocity dispersions on the dust disc parameters 68

7 Summary 71

8 Kokkuvõte (Summary in Estonian) 73

Bibliography 75

Acknowledgements 84

Attached original publications 85

Curriculum vitae 129

Elulookirjeldus 132

LIST OF ORIGINAL PUBLICATIONS

This thesis is based on the following publications:

I **R. Kipper**, E. Tempel, A. Tamm 2012, "Kinematic modeling of distant galaxies", Baltic Astronomy 21, 523

II E. Tempel, A. Tamm, **R. Kipper**, P. Tenjes 2015, "Recovering 3D structural properties of galaxies from SDSS-like photometry", Research in Astronomy and Astrophysics 15, 1613

III **R. Kipper**, P. Tenjes, O. Tihhonova, A. Tamm, E. Tempel 2016, "Stellar kinematics using a third integral of motion: method and application on the Andromeda galaxy", Monthly Notices of the Royal Astronomical Society, accepted for publication

Other related publications of the dissertant:

IV E. Tempel, A. Tamm, M. Gramann, T. Tuvikene, J. Liivamägi, I. Suhhonenko, **R. Kipper**, M. Einasto, E. Saar 2014, "Flux- and volume-limited groups/clusters for the SDSS galaxies: catalogues and mass estimation", Astronomy and Astrophysics 566, A1

V E. Tempel, Q. Guo, **R. Kipper**, N. I. Libeskind 2015, "The alignment of satellite galaxies and cosmic filaments: observations and simulations", Monthly Notices of the Royal Astronomical Society 450, 2727

VI E. Tempel, **R. Kipper**, A. Tamm, M. Gramann, M. Einasto, T. Sepp, T. Tuvikene 2016, "Friends-of-friends galaxy group finder with membership refinement. Application to the local Universe", Astronomy and Astrophysics 588, A14

Author's contribution to the publications

Author's research has given an essential contribution to all these publications. The author's contribution to the original publications is indicated below. The Roman numerals correspond to those in the list of publications.

Publication I. The author prepared all the data for the calculations and calculated the photometric model parameters and kinematic quantities of the galaxies. He made all the figures and wrote most of the draft of the paper.

Publications II. The author prepared the test-galaxy set for further modelling and contributed to writing the paper.

Publications III. The author did the calculations for the dynamical model presented in the paper. Similarly, the author prepared the manuscript, completed the figures and wrote the text.

Publication IV. The author's part in the given paper was to test and prepare the publication of the catalogue data.

Publication V. The author contributed to the interpretation of the results and made all the figures in the paper.

Publication VI. The author implemented the refinement method of the groups detection and prepared the pertinent figures and text. He was responsible for testing and preparing the published catalogue.

THE NOMENCLATURE OF THE USED VARIABLES

Symbol	Description
x_i, v_i	Cartesian coordinates and velocities in that direction; $i = \{1, 2, 3\}$
R, θ, z	cylindrical coordinates: radius, azimuthal angle and the distance from R-θ plane
ξ_1, ξ_2	elliptical coordinates (see Eq. (2.24) and (2.25))
z_0	the focal length of the elliptical coordinates
l_i	spacial luminosity density of i-th component of the galaxy
ρ_i	spacial density of i-th component of the galaxy
L_i	total luminosity of i-th component of the galaxy
M_i	total mass of i-th component of the galaxy
ρ_0, ρ_c	central density and density at a_c of Einasto profile
a_0, a_c	harmonic mean radius and half-light radius of Einasto profile
h, k	normalizing constants, found in Eq. (4.5)
N	parameter describing the shape of Einasto profile
d_N	normalizing constant depending on N
X, Y	apparent major and minor axis coordinates of a galaxy projected to the plane of the sky
X_0	horizontal axis of observed image
A	semi-major axis of equidensity line in model image
$I(v), I(X, Y, v)$	velocity distribution
γ	inclination angle of the galaxy (90° is edge-on)
ϵ	position angle measured from the major axis (X_0) counterclockwise
κ_d	dust attenuation coefficient
τ	optical depth along the line of sight
τ_0	optical depth seen in a face-on galaxy through the center
z_d	scale height of the dust disc (see Eq. (6.1))
R_d	scale length of the dust disc (see Eq. (6.1))
σ_R, σ_θ, σ_z	velocity dispersion in radial, azimuthal and vertical direction
Ψ	phase space density
I_1, I_2, I_3	integrals of motion
k_θ, k_z	the shape parameters of velocity ellipsoid, see Eqs. (2.7) and (2.6)
ζ	function describing orientation of the velocity ellipsoid, see Eq. (2.5)
κ, ξ	variables used for brevity in Jeans equations, see Eqs. (2.10) and (2.11)
p, g	variables used for brevity in the Jeans equations, see Eqs. (2.38) and (2.39)
a_2, b_2	parameters that constrain the shape of the velocity ellipsoid

INTRODUCTION

There is some curiosity in everyone and a desire to know what is inside various objects and how they work. In case of an earthly object it is at least theoretically possible to break it apart and find out; for more distant ones, such as stars and galaxies, one can only observe and guess. This kind of curiosity has led to many great discoveries, which have helped to both confirm and reject our views of the world. Here are two examples of how astronomy has helped other branches of physics. First, it was known that stars should have an unknown source of energy that cannot be caused either chemical burning or gravity. Curiosity to understand the nature of the energy source supported the development of nuclear physics. Second, there was a kind of inconsistency in the motion of the planet Mercury indicating that the gravity theory was not ready yet. Explaining the inconsistency led to the development/confirmation of the general theory of relativity. These discoveries were made thanks to the uniqueness of astronomy: the conditions in space are so rare and uncommon, that they cannot be mimicked in laboratories, making astronomy one-of-a-kind testing field for existing theories.

Even at present, we are witnessing an inconsistency with common knowledge and may be at the brink of a discovery: we have seen that there must be some kind of dark matter and dark energy, which needs to be explained. The understanding of the nature of dark matter and dark energy constitutes the the fundamental problems of present-day astronomy.

The way to find the amount of dark matter is simple: look how much matter there is altogether, then subtract what you know and the rest is the dark matter. The known part consists of observable matter: stars, gas and dust, for which the mass can be estimated relatively easily from various kinds of observations. Stellar mass can be derived from spectral energy distribution of a stellar system, gas mass from spectral emission lines and dust mass from far infrared emission and absorption of light. The total amount of matter can be estimated by gravitational lensing, by the temperature measurements of hot X-ray gas, by dynamic modelling of the observed motions in galaxies and by the virial theorem. Some of these methods work better for finding masses in large scales (outer parts of galaxies and galaxy clusters), some in smaller scales (inner parts of galaxies) thus complementing each other.

In order make our contribution to one of the goals of astronomy – to locate and identify the dark matter – we need to decide which method to calculate the amount and distribution of the dark matter is best for us and if needed to modify it to make it work even better. Out of all the potentially suitable methods, the dynamic modelling seems the most promising: it can be applied from the smallest scales (stellar clus-

ters) to the largest scales (galaxy clusters), making it a "Jack of all trades" of mass estimators and allowing in this way to study the distribution of dark matter in most interesting scales.

There are some difficulties when trying to model the dynamics of a galaxy: one cannot get the spacial luminosity and density for similar galaxy components from photometric observations only, there is the degeneracy of inclination angle and the intrinsic flatness of galaxy, and there are difficulties when restoring the internal velocity distribution from line-of-sight directional measured velocities. In the present thesis, we study to what extent the third integral of motion can help to ease the difficulties and how much dust in external galaxies, convolution due to atmosphere and spectrograph slit width influence the kinematics.

This thesis is structured as follows. The first Chapter gives an overview of what dynamic modelling is, what can be derived from dynamic modelling and what has been done in this field. In the second Chapter we describe Jeans equations, how they can be solved with respect to gas and for stellar kinematics and how in case of stars to take into account the third integral of motion and the shape of the velocity dispersion distribution. The third Chapter is devoted to observational effects needed to consider when comparing calculated models with observations: the need to take into account all the emission along the line of sight, atmospheric smearing effects, dust attenuation inside a galaxy and distortion of kinematics due to used instruments and how to extract kinematical characteristics from spectra. The ways to derive spatial density distribution of a galaxy from photometric image fittings are described in the fourth Chapter. The application of the developed stellar and gas model for a sample of external galaxies is presented in Chapter five, where we see how our model fits with real observations. Chapter six describes how the presence of dust in galaxies changes the observed kinematical characteristics: rotational velocity and dispersions. The Thesis ends with a concluding Chapter.

CHAPTER 1
OVERVIEW OF DYNAMIC MODELLING

In the first chapter we give a brief overview of and acknowledge the contribution of past masters: what kind of dynamic modelling has been done and what are the different techniques in this field.

1.1 The importance of dynamic modelling

The advantage of dynamic modelling comes forth when we think that we know how mass is distributed inside a stellar system (e.g. galaxy, stellar association, galaxy cluster etc) and would like to know whether our understanding is correct. It is possible to check it with a general methodology of any dynamic modelling: first we create a priori mass distribution, solve necessary equations to calculate kinematical characteristics and compare the derived results with observations. In case of consistency our knowledge about the systems mass distribution is likely to be adequate, otherwise some changes to the mass distribution parameters are needed. One of the first examples were models leading to the discovery of a dark matter halo around the Andromeda galaxy from observations by Rubin & Ford (1970) – the calculated motions created by the visible stellar matter were not consistent with the observed ones, therefore, an unknown component must be present – a dark matter halo (Einasto et al. 1974; Rubin et al. 1980). Detailed comparison of the model calculations with observations allow to constrain the distribution of unseen matter i.e. specify the density distribution parameters.

In addition to the mass determination in large scales, dynamic modelling provides the possibility to estimate the mass concentration also in the centres of galaxies and to provide arguments for the existence of supermassive black holes (Joseph et al. 2001; Cappellari et al. 2002; Devereux et al. 2003; Statler et al. 2004; Nowak et al. 2007; Gnerucci et al. 2011). Since the direct dynamical influence of supermassive black hole reaches less than a fraction of parsec around it, the surrounding luminosity smears the image and "blinds" us making the determination of the black hole mass and the surrounding matter density profile in the inner regions of a galaxy rather uncertain (Valluri et al. 2004). To overcome this disadvantage there have been developed alternative techniques (e.g. reverberation mapping and delays of polarisation of spectral lines (Afanasiev & Popović 2015)), allowing also to test the influence of central black holes in various dynamic models.

Dynamic modelling can be used also to study the origin of the scatter in fundamental plane (van Albada et al. 1995; Lanzoni & Ciotti 2003; Riciputi et al. 2005;

Cappellari et al. 2006). The fundamental plane is a relation between the observables of elliptical galaxies and it ties sizes, velocity dispersions and luminosities (masses) of galaxies – the same parameters as dynamic modelling. Thus, it is not surprising that this kind of modelling was found to be an excellent tool to calculate constraints and scattering of the fundamental plane.

Another application of dynamic modelling is to remove or to decrease some degeneracies that exist in pure photometric modelling. For example, the intrinsic flatness of a galaxy component may originate either from rotation or from anisotropy of the velocity dispersions. As both of them are stable states of a galaxy (Davies et al. 1983; Statler et al. 2004), dynamic modelling provides the means to distinguish the origin of flatness (Satoh 1980; Binney et al. 1990) and quantify the amount of rotation.

Thus, there are many goals that dynamic modelling helps to achieve, however, there are also drawbacks. One general problem of the dynamic modelling is the degeneracy between the anisotropy of the velocity dispersion distribution with the density distribution. Due to the degeneracy, it is possible to generate very similar integrated over the line of sight velocity profiles with different density distributions and intrinsic velocity dispersions (Merrifield & Kent 1990). As neither the density nor velocity dispersion distribution are known perfectly, model construction remains incomplete. Hence, it is crucial to try to develop new dynamic models until we are able to solve or to decrease the degeneracy.

1.2 Overview of dynamic modelling

We may distinguish four general methods for modelling: phase density modelling, the use of Jeans equations, Schwarzschild orbit superposition modelling and N-body simulations. In this section we will see how they work and also consider the advantages and disadvantages of these methods.

1.2.1 Models based on the phase density distribution

The most complete description of a stellar system is given by the phase density distribution Ψ (the density of particles in ordinary and velocity space). Corresponding analytical and semianalytical methods include the finding of a phase density distribution consistent with the collisionless Boltzmann equation.

As the ordinary density distribution is the integral of the phase density distribution over the velocities, it is possible to calculate the phase space as the inverse of the previous relation – the corresponding equation is called Eddington equation or Eddington inversion formula. This approach is very general, but its application still has some constraints due to the need to be consistent with the Boltzmann equation:

the birth and death rate of particles (stars) must be equal inside the system, or at least to be small[1]. Next, there should be no correlation between the locations of the stars, which is doubtful in case of density waves and spirals[2]. In addition, solving the Eddington equation is difficult since the number of variables is usually higher than the number of available equations.

The phase density modelling simplifies remarkably, when we take into account the Jeans theorem stating that the phase density of a steady state galaxy is a function of integrals of motion instead of being a function of phase coordinates.The number of integrals of motion in a galaxy where orbits are regular is probably three. The proof of this statement is that six independent variables of the phase density can be described by action–angle variables (a coordinate system where motions are described by constant phase speed and oscillations). If the orbit averaging theorem holds, each action space element should contain angle variables in the same way, which removes the angle variable from phase density and makes the phase space density a three-variable function thus confirming the existence of only three integrals of motion (Binney & Tremaine 2008).

When the ordinary mass densities are calculated from the phase space densities via integration, an analytical form of density distribution and also some kind of symmetry of a system are usually assumed. Common assumptions are spherical symmetry and axisymmetry. Perhaps the most important phase density model in case of a spherical stellar systems is the Osipkov–Merritt model. In this model the phase space density is assumed to be only a function of energy and angular momentum integrals, and a specific function form was used allowing also analytical calculations. Osipkov–Merrit model was used by e.g. Carollo et al. (1995), (Ciotti et al. 1996), (Meza & Zamorano 1997), (Łokas & Mamon 2001), (Baes & van Hese 2007), (Ciotti et al. 2009). Other commonly used models are polytopes (Saxton & Ferreras 2010), isothermal sphere, double power law models etc. The stability of these models (especially Osipkov–Merritt models) has been checked both analytically (Hjorth 1994) and numerically by Meza & Zamorano (1997) and criteria for stability were formulated (Meza & Zamorano 1997). For axisymmetric phase space models there are only a few analytical solutions. One of them worth to mentioning is an isotropic rotator model where velocity distribution is assumed to be isotropic everywhere and all the flattening of a galaxy originates from rotation. Modern methods use multicomponent approximations, such as developed by Baes & van Hese (2007), who combined multiple anisotropy profiles to achieve arbitrary density and kinematical distribution.

Here we enlist a few examples that have been conducted with phase space density modelling in spherically symmetric cases: Van Hese et al. (2009) used phase density

[1]This is satisfied for low mass stars, but less so for high mass stars.

[2]This does not influence modelling too much when the amplitude of the density waves is small.

to constrain the velocity dispersion anisotropy distribution by assuming known relations for dark matter density distribution ($\rho/\sigma^3 \sim r^{-\alpha}$ relation[3] and $\beta - \gamma$ relation[4]); Carollo et al. (1995) assumed the γ model for the matter density distribution and Osipkov-Merritt anisotropy distribution to find a relation between the central density slope and the anisotropy radius.

As a last remark on this point, the calculations in this kind of models involve integration over velocities one needs to demand that integrals of motion remain conserved quantities: energy in case of spherically symmetric galaxy, energy and angular momentum in case of axial symmetry. When intending to solve equations in more general cases, difficulties arise.

1.2.2 Modelling based on the Jeans equations

Modelling based on phase densities and on Jeans equations differ from each other by a technical approach. Phase space density modelling assumes energy conservation, a form of the gravitational potential (and therefore density) and an integral equation is solved to calculate velocities. Modelling based on Jeans equations assumes only density distribution and solves a differential equation system to calculate velocities. Intrinsically, both methods are based on the collisionless Boltzmann equation, and thus the given approaches may be considered equivalent. In case of phase space modelling, one has to assume a form of the arguments in the phase space density, but there is no need for it in case of modelling with Jeans equations. On the other hand, if we have a solution to the Jeans equations (i.e. the mean and the dispersion of the velocity), there is the drawback of not having any information on the higher moments of the velocity distribution – an information that phase space modelling can, in principle, provide.

The derivation of the Jeans equations starts from the Boltzmann collisionless equations:

$$\frac{\partial \Psi}{\partial t} + v_i \frac{\partial \Psi}{\partial x_i} + \frac{\partial v_i}{\mathrm{d}t} \frac{\mathrm{d}\Psi}{\partial v_i} = 0, \tag{1.1}$$

where $\Psi(t, x_1, x_2, x_3, v_1, v_2, v_3)$ is the phase space density, x_i and v_i are the Cartesian coordinates and velocities. By multiplying the Boltzmann equation with a velocity component and integrating it over the velocities we get a general form to the Jeans equations

$$\rho \frac{\partial \overline{v_j}}{\partial t} + \rho \sum_{i=1}^{3} \overline{v_i} \frac{\partial \overline{v_j}}{\partial x_j} = -\rho \frac{\partial \Phi}{\partial x_j} - \sum_{i=1}^{3} \frac{\partial (\rho \sigma_{ij}^2)}{\partial x_i}, \tag{1.2}$$

[3] relation $\rho/\sigma^3 \sim r^{-\alpha}$ ties the radial dependence of the density and radial velocity dispersion.

[4] β–γ relation ties anisotropy of the velocity dispersion and the logarithm of the density slope.

where ρ denotes density, Φ gravitational potential, and σ_{ij}^2 velocity covariance matrix defined by

$$\sigma_{ij}^2 = \overline{(v_i - \overline{v_i})(v_j - \overline{v_j})} = \overline{v_i v_j} - \overline{v_i}\,\overline{v_j}, \quad i,j \in \{1,2,3\}. \tag{1.3}$$

Henceforth we denote the part of the velocity dispersion tensor describing velocity dispersions in the meridional plane as the velocity ellipsoid. Each of the resulting Jeans equation contains four terms: the first describes the time variability of a system, the second the motion of the matter, the third the gravitational force and the fourth term of the equation describes the pressure gradient of the system. Altogether there are three Jeans equations, each describing motions in a certain direction.

Solving the Jeans equations poses some difficulties: the number of variables is larger than the number of equations, even if we add the Poisson equation $\nabla^2\Phi = 4\pi G\rho$. This means that it is necessary to assume additional constraints for solving them. Most commonly, an assumption about time evolution and the shape of a galaxy are used – galaxies are assumed to be stationary with a spherical or axisymmetric shape.

Models with spherical symmetry

When assuming spherical symmetry, the number of Jeans equations is one as other two equations turn into identity. Nevertheless, there are still more unknown variables than one, and thus even in this case some additional assumptions are needed. The most common assumptions for spherical systems are isotropic velocity distribution or the distribution described by Osipkov-Merritt model.

When computational power and observational possibilities were still developing, there was motivation to solve Jeans equation for a one-component model and use similar galaxies for comparison. Models with the Jaffe and Hernquist density distribution profiles with isotropic velocity distribution were developed by Jaffe (1983) and Hernquist (1990), respectively. Dehnen density distribution profile was introduced and Jeans equation was solved by Dehnen (1993), for Navarro-Frenk-White density distribution profile, the most commonly used one to describe the dark matter halo, Jeans equation was solved by Łokas & Mamon (2001) assuming a different velocity anisotropy assumption.

An analytical solution for a two-component model usually contains a stellar component and a supermassive black hole or a dark matter halo. Jeans equation with a Dehnen profile component and a central supermassive black hole was solved as system by Tremaine et al. (1994); double Hernquist model with Osipkov-Merritt velocity anisotropy was solved analytically by Ciotti (1996). Ciotti et al. (2009) constructed also a solution for a Dehnen density profile with total matter distribution being proportional to r^{-2}. Magorrian et al. (1998), (Cretton & van den Bosch 1999), (Drehmer

et al. 2015) provided examples for applying the model with supermassive black hole kinematics. A simple application for the dark matter distribution was provided by Dehnen et al. (2006), but usually researchers have aimed for more elaborate models, taking into account also additional data from N-body simulations (e.g. β–γ relation).

A considerable amount of effort has been made to find why the $\beta - \gamma$ relation holds. Based on Jeans equations, Zait et al. (2008) found that deprojected Sersic density distribution profile affords better agreement with the $\beta - \gamma$ relation than Navarro-Frank-White (NFW) profile. An & Evans (2009) used Jeans equations and $\beta - \gamma$ relation and derived that central density of a galaxy must fall slower than r^{-2} constraining the existing model remarkably. For dark matter halos there is also a $\rho/\sigma_R^3 \sim r^{-2}$ relation giving interesting insights into dynamics (Dehnen & McLaughlin 2005; Hunter 2014).

One approach to remove the necessity of additional constraints for the Jeans equations was introduced by Merrifield & Kent (1990), who generalised the Jeans equations to higher velocity moments. However, applying the method requires rather good quality velocity distribution observations. Nevertheless, Łokas (2002) showed that at least in case of dwarf galaxies this kind of modelling has a perspective.

To generalise Jeans equations for spherical systems, Schmidt et al. (2009) included a small amount of rotation while maintaining its density and velocity dispersion distribution as much as possible.

A practical result for spherical galaxies comes from Binney & Mamon (1982) who calculated the anisotropy and the radial velocity dispersions for a non-rotating galaxy. Density distribution was derived from surface brightness distribution by assuming a certain mass-to-light ratio, line of sight velocity dispersions were taken from observations. This work demonstrated that the solution can be found without assuming any specific density or anisotropy profile.

Models with axial symmetry

Another widely used geometrical simplification to solve the Jeans equations is the assumption of the axial symmetry of a galaxy (all the galaxies modelled in this thesis use this assumption). After applying the corresponding constraints we have two Jeans equations as the equation describing motions in rotational direction becomes identity.

The more complicated the system becomes, the more difficult it is to solve. For this reason it is not surprising that when compared to analytical solutions in spherical case, there are only few analytical solutions in axisymmetric case. One of them is derived by Smet et al. (2015), who solved Jeans equations for logarithmic potential (for describing the dark matter) combined with Myamoto-Nagai density distribution (for describing the stellar profile) with isotropic velocity dispersion distribution. Chosen Myamoto-Nagai profile allowed to vary bulge to disc ratio within a dark matter halo.

Emsellem et al. (1994) found a solution to Jeans equations for a density profile consisting of several Gaussian distributions (multi–Gaussian expansion). This method was applied to several galaxies by Cappellari et al. (2015). A method to solve Jeans equations in a case when the velocity ellipsoid is not aligned with coordinates and assuming of a form for the third integral of motion was developed by Tempel & Tenjes (2006).

An advantage to study flattened discs is that in radial direction the mass density and gravitational potential change more slowly than in vertical direction. In this case the system of two equations reduces to two independent equations near the galactic plane. Hence, to study the vertical structure of discs, sometimes only the vertical Jeans equation is used. For example, Zhao et al. (2006) assumed exponential density distribution in vertical direction and solved Jeans + Poisson equations to get the structural parameters of a disc. The use of the vertical Jeans equation has an advantage when we cannot see the entire galaxy, but just part of it. For our Galaxy, the observations cover only the Solar neighbourhood and we can construct corresponding models for a small part of a Galaxy and in vertical direction. The vertical Jeans equations have been used to derive the amount of local dark matter density (Holmberg & Flynn 2004; Bovy & Tremaine 2012; Moni Bidin et al. 2012; Sánchez-Salcedo et al. 2016). The general conclusion is that there is only little dark matter in Solar neighbourhood. The reason of this is not very clear. There are suggestions that the virialisation prerequisite of the collisionless models is not fulfilled (Garrido Pestaña & Eckhardt 2010), hence this type of modelling may not be completely justified. On the other hand, Sánchez-Salcedo et al. (2011) and Candlish et al. (2016) re-estimated it to be usable approximation, but with the concern that radial dependence of density might affect the validity of discarding the radial Jeans equations in the assumptions.

In the process of modelling of the kinematics of disc galaxies, there are some setbacks that have led to the necessity to develop more sophisticated models. Satoh (1980) showed that isotropic velocity dispersion tensor is not enough to describe the motions in a rotating elliptical galaxy, thereby stressing the need to use anisotropic velocity distribution. Binney et al. (1990) tried to model the kinematics of flattened elliptical galaxies by using axisymmetric Jeans equations and found that in several cases the existence of a third integral of motion is necessary i.e. the velocity ellipsoid should be three-axial.

We saw that for axisymmetric galaxies there are several methods to solve Jeans equations. There is also a plethora of applications. Here is a selection of the uses: to explain the discrepancies between the circular velocities and the observed rotational velocities (Cinzano et al. 1999; Corsini et al. 1999; Young et al. 2008), to calculate the mass-to-light ratios (Statler et al. 1999; Cappellari 2008), and to find the hidden discs inside elliptical galaxies (Rix & White 1992; Cinzano & van der Marel 1994).

1.2.3 Models based on the Schwarzschild orbit superposition

One promising approach to study the structure and dynamics of a galaxy is to model a galaxy as a superposition of individual stellar orbits. If density or equivalently gravitational potential distribution is known, it is possible to convert it to the Laplacian/Hamiltonian allowing the calculation of the orbits of stars in a galaxy. Once a substantial amount of orbits has been calculated (orbit library), it is possible to give to each orbit a weight to achieve initial density distribution. This is usually done by maximising entropy. Schwarzschild (1979) was the first to develop and use such a technique for modelling the kinematics of a galaxy. With the natural byproduct of the model we have quite complete kinematical description of a galaxy allowing the comparison of the model with observed kinematics.

Such a great modelling scheme does not come without drawbacks, there are some cases, when projecting the galaxy, the orbit superposition creates a line/point which could be an artefact unseen in realistic galaxies. This problem is called the fold/cusp catastrophe and needs to be taken into account. Another problem is that the calculation of the orbit library is rather time consuming. In some cases this can be overcome when reusing orbits from a similar potential. An interesting possibility to achieve a higher precision in numerical orbit integration is to combine Schwarzschild method with Jeans equations as it was described by Jalali & Tremaine (2011). Another possibility is to use the action–angle variables when calculating the orbit library (Binney & McMillan 2016).

When comparing the Schwarzschild superposition method with Jeans equations based methods, the first one has an advantage, namely a possibility to model stellar motions in three-dimensional potential. From Schwarzschild modelling it was concluded by van de Ven et al. (2008) that the observed kinematics of an elliptical galaxy can be well described by three-axial density distribution. In some cases only a central part of a galaxy can be described in that way allowing the calculation of the masses of supermassive black hole in the centres of galaxies (van der Marel et al. 1998; Cretton & van den Bosch 1999; Cretton et al. 1999; Onken et al. 2014).

Here are also a few additional concise examples for the uses of Schwarzschild modelling: Cappellari et al. (2007) used three-integral Schwarzschild model to relate anisotropy in the V/σ-flatness plane with the flattening of the velocity ellipsoid; Cappellari et al. (2006) used both two-integral Jeans equations and three-integral Schwarzschild modelling to find that mass-to-light ratios are similar in both cases, indicating good consistency between both methods.

1.2.4 Numerical simulations of galaxy dynamics

Numerical simulations have the highest flexibility when compared to other dynamic modelling methods: they are able to simulate spirals, bars, global asymmetries in galaxy forms, expansion and contraction of discs, mergers, instabilities etc. Despite their numerous advantages, simulations also have some downsides: we do not know initial conditions for simulations, there exists numerical instability, and close encounters between stars (where forces tend to infinity) are not properly taken into account. However, there are also excellent algorithms to overcome several numerical difficulties (e.g. leapfrog integration, tree-code to find potential etc).

Mostly, numerical simulations are used to study non-axisymmetric components of galaxies, such as bars, spirals, stellar streams etc (Vera-Ciro et al. 2014; Molaeinezhad et al. 2016; Grand et al. 2016) or nonstationary processes in galaxies, such as relaxation, mergers etc (Ida et al. 1993; Sparre & Hansen 2012; Sellwood 2013). Numerical simulations also provide an excellent testing ground for the stability and consistency of different methods. For example, Meza & Zamorano (1997) found a stability criterion for dynamic model with Dehnen profile and Osipkov-Merritt anisotropy; Malvido & Sellwood (2015) studied the stability of three-axial dark matter halo and found it to be stable for 100 dynamic timescales.

There have been some attempts to combine the advantages of different methods. For example Yurin & Springel (2014) used Schwarzschild method to obtain a realisation of a stable N-body snapshot that satisfies Boltzmann collisionless equation.

CHAPTER 2
MODELLING THE DYNAMICS OF A GALAXY WITH THE JEANS EQUATIONS

In the previous chapter we discussed different methods one can use to model the dynamics of a galaxy. In this chapter we turn our attention to the Jeans equations, which to some extent constitute the main equations of this thesis, and solve them with assumptions describing either a gaseous or a stellar component.

2.1 Jeans equations in a general form

The most general equation describing the dynamics of a N-body system is the Boltzmann equation (1.1). For practical dynamical fitting, it is sometimes considered too general to use since it contains a non-observable quantity – the phase density (Ψ). Instead, the moment equations of the collisionless Boltzmann equation – the Jeans equations (1.2) – are commonly used. The Jeans equations tie together ordinary mass density (ρ), matter velocity (v_i), gravitational potential of the whole system (Φ), and the velocity covariance matrix (usually called velocity dispersion tensor or velocity ellipsoid) defined by Eq. (1.3). They were first derived and used for astronomical purposes by Jeans (1915), after whom they are named.

There are certain assumptions that are quite common in most studies conducted in the field of dynamical modelling. The first assumption is stationarity, i.e. all time derivatives of the density are taken to be zero[1]. Secondly, the galaxy is assumed to be either spherically or axially symmetric. The assumption of the spherical symmetry is more difficult to validate from observations, however, the assumption about axial symmetry approximation is supported by observations. For example, Takeuchi et al. (2015) showed that the average intrinsic roundness (axial ratio in $z = 0$ plane) of the disc population at redshift ~ 0.5 is 0.92 ± 0.05 indicating the axial symmetry to be a good assumption for disc galaxies[2] even at moderate redshifts.

In the present thesis we assume the galaxies to be stationary and have axial symmetry. Thus, when comparing the model calculations and real galaxies we select

[1] In some cases, it is possible to neglect this assumption and to study the evolution of the galaxy (Falco et al. 2013), but it requires some additional simplifications that might not describe a realistic galaxy.

[2] In case of a slightly irregular galaxy, the gravitational potential is smoother and rounder than observed luminosity distribution (potential can be thought as the density which is smoothed by r^{-1} kernel), making the dynamical modelling possible, but slightly less reliable.

galaxies with regular velocity fields. In this case cylindrical coordinates (R, θ, z) are convenient to use.

In case of axial symmetry with respect to the z-axis the velocity dispersion in the rotational direction is independent of the vertical and radial velocity dispersions. Mathematically it is noted as

$$\sigma^2_{R\theta} = \sigma^2_{z\theta} = 0. \tag{2.1}$$

The general form for the Jeans equation with our assumptions are

$$\frac{\partial(\rho\overline{v_R^2})}{\partial R} + \frac{\partial(\rho\overline{v_R v_z})}{\partial z} + \rho\left(\frac{\overline{v_R^2} - \overline{v_\phi^2}}{R} + \frac{\partial\Phi}{\partial z}\right) = 0 \tag{2.2}$$

$$\frac{1}{R^2}\frac{\partial(R^2\rho\overline{v_R v_\phi})}{\partial R} + \frac{\partial(\rho\overline{v_z^2})}{\partial z} + \rho\frac{\partial\Phi}{\partial z} = 0. \tag{2.3}$$

Our assumptions do not constrain the mixed component of the velocity dispersion tensor in the meridional (R–z) plane. For better interpretation we describe the mixed component of the velocity dispersion tensor with the orientation angle and the flatness. We denote α as the angle between the galactic plane and the axis of the velocity ellipsoid, which can be converted to the third mixed component of the velocity dispersion tensor (see Fig 2.1) by using the following formulae:

$$\sigma^2_{Rz} = \zeta(\sigma^2_{RR} - \sigma^2_{zz}), \tag{2.4}$$

$$\text{where} \quad \zeta = \frac{1}{2}\tan 2\alpha. \tag{2.5}$$

The shape of the velocity ellipsoid is described with axial ratios

$$k_z \equiv \sigma^2_z/\sigma^2_R, \tag{2.6}$$

$$k_\theta \equiv \sigma^2_\theta/\sigma^2_R. \tag{2.7}$$

Hereinafter we are denoting $\sigma^2_z \equiv \sigma^2_{zz}$, $\sigma^2_R \equiv \sigma^2_{RR}$, and $\sigma^2_\theta \equiv \sigma^2_{\theta\theta}$ for brevity.

After taking all this into account, we have the following form of the Jeans equations:

$$\frac{\partial(\rho\sigma^2_R)}{\partial R} + \left(\frac{1-k_\theta}{R} + \frac{\partial\kappa}{\partial z}\right)\rho\sigma^2_R + \kappa\frac{\partial(\rho\sigma^2_R)}{\partial z} = -\rho\left(\frac{\partial\Phi}{\partial R} - \frac{V^2_\theta}{R}\right), \tag{2.8}$$

$$\frac{\partial(\rho\sigma^2_z)}{\partial z} + \left(\frac{\xi}{R} + \frac{\partial\xi}{\partial R}\right)\rho\sigma^2_z + \xi\frac{\partial(\rho\sigma^2_z)}{\partial R} = -\rho\frac{\partial\Phi}{\partial z}. \tag{2.9}$$

Here

$$\kappa \equiv \zeta(1-k_z), \tag{2.10}$$

$$\xi \equiv \kappa/k_z, \tag{2.11}$$

and V_θ is the rotation velocity of a galaxy. The gravitational potential and density are related with the Poisson equation

$$\nabla^2\Phi = 4\pi G\rho. \tag{2.12}$$

The Jeans equation describing the motions in the θ direction became identity due to the assumption of axial symmetry.

The main equations in this thesis (2.8, 2.9) are used for the dynamical modelling and contain altogether seven free functions: the density distribution ρ, the overall gravitational potential Φ, rotational velocity V_θ, velocity dispersions $\sigma_R^2, \sigma_z^2, \sigma_\theta^2, \sigma_{Rz}^2$. We describe the velocity dispersion tensor by radial velocity dispersion σ_R^2 (i.e. the amplitude of velocity dispersion) and the variables describing the shape (k_z, k_θ) and orientation (α, or equivalently, ζ) of the velocity ellipsoid. In this thesis we assume that the density distribution is known a priori or calculated from surface photometry distribution and/or from the kinematics of different components (e.g. from gas motions). The Poisson equation allows the calculation of the gravitational potential from the density. The kinematical quantities we solve equations for are the rotational velocity and velocity dispersions. One can see that the number of Jeans equations is smaller than the number of variables, therefore solving for the kinematics requires additional assumptions, which are dependent on the nature of the component.

2.2 Modelling the dynamics of a gas component in a galaxy

The gas dynamics can be handled as a special case of a more general stellar dynamics. In our context (when ignoring gas viscosity) the main difference between the gas and the stellar dynamics is the frequency of collisions between gas particles. Each collision between atoms/molecules scatters both particles in a random direction, hence making the velocity ellipsoid rounder. Also, when atoms form molecules and photodissociation causes molecules to disintegrate, the initial velocities of the particles are randomised, supporting the increase of isotropy. One process, which may create anisotropy for gas, is the extraction of gas from stars via stellar winds: the gas around a star has similar kinematic properties as the star, including velocities. When gas is removed slowly from the star, it retains the star's motion for a while and therefore shifts the kinematics of gas toward the stellar one. Fortunately, the collisions between the gas particles happen more frequently than the extraction of gas, making the gas velocity dispersion roughly isotropic.

In case of isotropic velocity distribution

$$k_z = k_\theta = 1, \tag{2.13}$$

therefore $\kappa = 0$ and $\xi = 0$. This simplifies Jeans equations remarkably, giving

$$\frac{\partial(\rho_{\rm gas}\sigma^2_{\rm gas})}{\partial R} = -\rho_{\rm gas}\left(\frac{\partial\Phi}{\partial R} - \frac{V^2_\theta}{R}\right), \tag{2.14}$$

$$\frac{\partial(\rho_{\rm gas}\sigma^2_{\rm gas})}{\partial z} = -\rho_{\rm gas}\frac{\partial\Phi}{\partial z}. \tag{2.15}$$

As pointed out by Binney & Tremaine (2008) these equations are analogous to the Euler equations in fluid dynamics with the term $\rho_{\rm gas}\sigma^2_{\rm gas}$ corresponding to the pressure. Velocity dispersion and the rotation velocity of the gas as a function of coordinates (R, z) result from these expressions in a quite straightforward way

$$\sigma^2_{\rm gas}(R,z) = \frac{1}{\rho_{\rm gas}}\int_z^\infty \rho_{\rm gas}(R,z')\frac{\partial\Phi(R,z')}{\partial z'}{\rm d}z', \tag{2.16}$$

$$V^2_{\rm gas}(R,z) = \frac{R}{\rho_{\rm gas}}\left[\frac{\partial(\int_z^\infty \rho_{\rm gas}\frac{\partial\Phi}{\partial z'}{\rm d}z')}{\partial R} + \rho_{\rm gas}\frac{\partial\Phi}{\partial R}\right]. \tag{2.17}$$

An important difference between the solutions of the Jeans equations for gaseous and stellar components (see Sect. 2.3) is our ability to calculate rotation velocities without further assumptions. Although this is a good advantage, there is a drawback as in using these equations we need to know the gas density distribution – a quantity that is difficult to derive from observations[3].

2.3 Modelling the dynamics of a stellar component

The main difference between the stellar and gas dynamics lies in the shape of the velocity ellipsoid: in case of stellar dynamics we cannot assume isotropy as we did with the gas component – stars are effectively collisionless and there is no dominant mechanism that makes velocity distribution rounder. The anisotropy makes the closing of the Jeans equations impossible by themselves and to solve them one needs to find additional relations. In this section we will study the shape of the velocity ellipsoid and constrain it with the help of the third integral of motion. The latter gives us additional information to close the Jeans equation and make the system solvable.

2.3.1 Tri-axiality of the stellar velocity dispersions

According to one or two-integral models, the velocity dispersion of the stellar component of a galaxy is isotropic or two-axial. There are both observational and com-

[3]The difficulty arises from undetermined chemical composition and physical state of the gas.

putational indications that support tri-axial velocity dispersions and therefore suggest the need for more complex models.

Observationally, the most accurate velocity dispersions can be calculated from the best quality data i.e. for the Solar neighbourhood: we can measure the distances and 3D velocities of nearby stars and construct the velocity distribution. It has been done using HIPPARCOS (ESA 1997) observations by Dehnen (1998), who measured the $\sigma_R : \sigma_\theta : \sigma_z = 1 : 0.6 : 0.35$ using the proper motions of 14 369 stars. When GAIA (Perryman et al. 2001) mission will be completed, more accurate velocity ellipsoid can be measured inside a large part of our Galaxy. Another approach is to use only the radial velocities of stars. Such work was done by Smith et al. (2012) who used observations of the SDSS Stripe 82 and found ratios of the velocity dispersions $0.7 < \sigma_\theta/\sigma_R < 0.9$ and $0.55 < \sigma_z/\sigma_R < 0.75$. The accuracy of the velocity ellipsoid has been estimated, in addition to statistical error, by measuring how much various effects of our Galaxy influence the shape of velocity ellipsoid. Minchev & Quillen (2007) estimated the error in Oort constants, which are directly related to velocity ellipsoid, due to density wave to be in order of 5 km s^{-1}, making the error of σ_θ in between $5 \ldots 10$ km s^{-1}. The latter result indicates that the shape of the velocity ellipsoid is not very sensitive to the perturbations caused by density waves. The tilt α of the velocity ellipsoid is changing with the height from the galactic plane and with the stellar population (Dehnen & Binney 1998; Smith et al. 2012; Büdenbender et al. 2015) mainly in the range of $5 \ldots 20^\circ$. There have been attempts to study the velocity ellipsoid in other galaxies (Bottema 1993; Gerssen et al. 1997; van der Kruit & de Grijs 1999), but these studies contain substantial assumptions about these galaxies. Nevertheless, their conclusions show that the velocity ellipsoid form in other galaxies has similarities with the ellipsoid in the Solar neighbourhood.

The tri-axial velocity ellipsoid has been proposed also as a solution of the last parsec problem. The last parsec problem is an issue when two supermassive black holes orbit each other, but do not merge (from the theoretical point of view, it is difficult to find a mechanism for the system to lose angular momentum and make the black holes approach each other). Observationally binary black holes are extremely rare compared to galaxy merging events, therefore, the black holes have been merged and there is a contradiction between the observations and theory. The tri-axial velocity ellipsoid helps to solve the last parsec problem (Vasiliev & Athanassoula 2015) by allowing the system to lose angular momentum and eventually merge. In addition, the tri-axial velocity dispersion is needed to model the kinematics of flattened elliptical galaxies (Binney et al. 1990).

A considerable amount of information about the velocity ellipsoid has been found from Schwarzschild orbit superposition modelling (Valluri et al. 2004; van de Ven et al. 2008; Vasiliev & Athanassoula 2015), where the shape of the velocity ellipsoid

comes forth naturally when stacking the velocities of orbits going through a measured point. Schwarzschild orbits superposition method also favours the tri-axial velocity dispersion (Schwarzschild 1979). Cappellari (2008) provided us with a discussion on the basis of Schwarzschild method dataset how the velocity ellipsoid is oriented in galaxies. This study supported the approximation that the shape of the velocity ellipsoid is tri-axial and its alignment is along the axis of cylindrical coordinates. This approximation is sufficient for most cases.

There are studies of how distinct phenomena change the velocity ellipsoid of stars. Vorobyov & Theis (2008) made a two-dimensional simulation of spirals and found that the axis ratio of the velocity ellipsoid in the galactic plane is mostly between 0.6 and 0.9, except in the convex (outer) edge of spiral, where it can reduce to $0.25 \ldots 0.5$ showing substantial effect from strong spirals. How bar and spirals change the shape of the velocity dispersions in Milky Way like galaxy is studied by Minchev & Quillen (2006, 2007). In contrast with isolated galaxies that are typically studied, satellites are affected by the external gravitation: the tidal effects make the shape of a dispersion ellipsoid more elongated, as was shown by Vera-Ciro et al. (2014).

A semianalytical result was calculated by Kuzmin (1961) showing that for the galactic plane the $k_z^{-1} = k_\theta^{-1} + 1$ relation must be satisfied, but only in case of flat systems. In more general cases validity of the result is not clear.

An interesting approach is to study the velocity dispersion distribution between different galaxies: for galaxies that are face-on or edge-on for the observer, one can see approximately one or two components of the dispersion tensor respectively. Therefore, studying the components independently and connecting the overall distributions is possible as Bottema (1993) showed.

To sum up, it is important to include the tri-axiality of the velocity ellipsoid, or equivalently, the third integral of motion, in order to describe a realistic galaxy.

2.3.2 Constraining the velocity ellipsoid with a third integral of motion

The Jeans theorem states that integrals of motion are the solutions to collisionless Boltzmann equation. The strong Jeans theorem specifies this by stating that in general the number of these integrals is three. Two of them, the energy and the angular momentum

$$I_1 = v_R^2 + v_\theta^2 + v_z^2 - 2\Phi, \tag{2.18}$$

$$I_2 = Rv_\theta \tag{2.19}$$

satisfy naturally the condition for the integral of motion. In case of only two integrals of motion, an axisymmetric model must have two-axial velocity ellipsoid, which is in contradiction with observations. Hence, as the velocity ellipsoid is tri-axial the existence of a third integral of motion is necessary.

One possible additional integral of motion suggested by Lindblad in early 1930s (Lindblad 1934) is the total energy in the vertical direction ($I_3 = v_z^2 - 2[\Phi(R,z) - \Phi(R,0)]$). Unfortunately this solution only holds for thin discs. A more general approach was given by Kuzmin (1953, 1956), who proposed that a third integral of motion could be in form of

$$I_3 = a_{20}v_R^2 + 2a_{11}v_R v_z + a_{02}v_z^2 + a_{10}v_R + a_{01}v_z + a_{00}, \tag{2.20}$$

where a_{20}, a_{11}, a_{02} are coefficients not depending on v_θ, a_{01}, a_{10} are linear functions of v_θ, a_{00} is a quadric expression of v_θ. If the Stokes operator is applied to an integral of motion the result must be zero (i.e. I_3 is constant along an orbit). This condition allows to constrain the proposed form for the third integral of motion. Algebraic manipulation by Kuzmin (1953) has provided that I_3 must have a form

$$I_3 = (Rv_z - zv_R)^2 + z^2v_\theta^2 + z_0^2(v_z^2 - 2\Phi^*); \tag{2.21}$$

Φ^* satisfies equations

$$z_0^2\frac{\partial\Phi^*}{\partial R} = z^2\frac{\partial\Phi}{\partial R} - Rz\frac{\partial\Phi}{\partial z}, \tag{2.22}$$

$$z_0^2\frac{\partial\Phi^*}{\partial z} = (R^2 + z_0^2)\frac{\partial\Phi}{\partial z} - Rz\frac{\partial\Phi}{\partial R}, \tag{2.23}$$

and can be found by solving that system. z_0 is a constant with a dimension of length.

When introducing elliptical coordinates by demanding that velocity ellipsoid is aligned with these coordinate lines (see Fig. 2.1), it results that $\pm z_0$ are the positions of foci of coordinates. It is natural that we use elliptical coordinates when handling the velocity ellipsoid (the θ coordinate remains the same as in cylindrical coordinates). Conversion between elliptical coordinates and cylindrical ones is done by using the following formulae:

$$\xi_1^2 = \frac{1}{2}[\Omega + \sqrt{\Omega^2 - 4z^2z_0^2}], \tag{2.24}$$

$$\xi_2^2 = \frac{1}{2}[\Omega - \sqrt{\Omega^2 - 4z^2z_0^2}], \tag{2.25}$$

where $\Omega = R^2 + z_0^2 + z^2$ and the parameters $\pm z_0$ correspond to the foci of the elliptical coordinates (ξ_1, ξ_2). The coordinate transformation does not influence the θ-direction. As a result, our integrals of motion are turned to the following from

$$I_1 = v_1^2, + v_\theta^2 + v_2^2 - 2\Phi, \tag{2.26}$$

$$I_2 = Rv_\theta, \tag{2.27}$$

$$I_3 = \xi_1^2v_1^2 + \xi_2^2v_2^2 + \xi_1\xi_2v_\theta^2 - 2z_0^2\Phi^*. \tag{2.28}$$

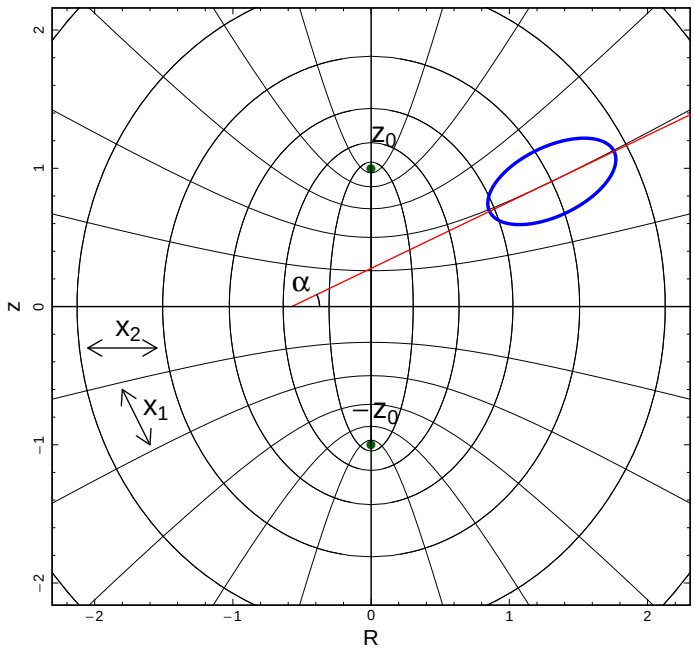

Figure 2.1: The illustration of the relation between cylindrical (R and z) and the elliptical coordinates (ξ_1 and ξ_2). α is the angle between the velocity ellipsoid (blue ellipse) and the galactic plane, $\pm z_0$ are the foci of the elliptical coordinates. The θ coordinate is perpendicular with the figure.

Einasto (1970) derived further and stricter constraints to the shape of the velocity ellipsoid by assuming that phase density $\Psi(\psi)$ is quadratic in respect to velocity components, which can be written by the integrals of motion:

$$\psi = a_1 I_1 + a_2 I_3 + 2\frac{b_1}{z_0} I_2 + \frac{b_2}{z_0^2} I_2^2. \tag{2.29}$$

As its Stokes derivative must be zero, the coefficients in front of each velocity component must be zero, which is only possible if the shape of the velocity ellipsoid is described by

$$k_{12}^* \equiv \frac{\sigma_{22}^2}{\sigma_{11}^2} = \frac{a_1' z_0^2 + a_2' \xi_2^2}{a_1' z_0^2 + a_2' \xi_1^2}, \tag{2.30}$$

$$k_{13}^* \equiv \frac{\sigma_{33}^2}{\sigma_{11}^2} = \frac{a_1' z_0^2 + a_2' \xi_2^2}{a_1' z_0^2 + a_2' z^2 + b_2' R^2}, \tag{2.31}$$

where the a_1', a_2' and b_2' are constants; the asterisk denotes that a variable is calculated by assuming the third integral of motion. Since the integrals of motion can be multiplied by a constant, we redefine the parameters by dividing them with a_1 i.e. $a_1' = 1$, $a_2 = a_2'/a_1'$ and $b_2 = b_2'/a_1'$. This removes one of the free parameters from the equations. The orientation of the velocity ellipsoid is conveniently given by

$$\zeta \equiv \frac{1}{2} \tan 2\alpha = \frac{Rz}{R^2 + z_0^2 - z^2}. \tag{2.32}$$

As we used here already cylindrical coordinates, we write the shape parameters of the velocity dispersion ellipsoid also in cylindrical coordinates as related with those in elliptical coordinates

$$k_z^* = \frac{\sin^2\alpha + k_{12}^*\cos^2\alpha}{\cos^2\alpha + k_{12}^*\sin^2\alpha} = \frac{\tan^2\alpha + k_{12}^*}{1 + k_{12}^*\tan^2\alpha}, \tag{2.33}$$

$$k_\theta^* = \frac{k_{13}^*}{\cos^2\alpha + k_{12}^*\sin^2\alpha} = \frac{k_{13}^*(1+\tan^2\alpha)}{1 + k_{12}^*\tan^2\alpha}. \tag{2.34}$$

To sum up, the velocity dispersion ellipsoid is determined in this model by three parameters: a_2, b_2 and z_0. The first two parameters describe the shape of the velocity ellipsoid, while the last one describes both its shape and orientation.

2.3.3 The solution of the Jeans equations and its consistency with the third integral of motion

Initially we had two Jeans equations but five unknown functions[4]. By using the third integral theory that allows to constrain the shape of the velocity ellipsoid we have now two unknown functions and three unknown constant parameters (a_2, b_2 and z_0). One unknown function is the rotational velocity, which we assume to be proportional with the circular velocity for each component:

$$V_\theta^2 = \beta^2 v_c^2 = \beta^2 R\frac{\partial\Phi}{\partial R}. \tag{2.35}$$

v_c denotes the circular velocity and β the proportionality factor.

The Jeans equations are coupled first order partial differential equations which in general are not analytically solvable. Since we are using the third integral approximation, we have an analytic form for k_z and k_θ, allowing to remove the coupling and turn the system into two separate first order partial differential equations. These are solved by the method of characteristics. Assuming we know the velocity ellipsoid shape from some other data, the resulting solution to the Jeans equations (2.8) and (2.9) are

$$\sigma_R^2(R,z) = \frac{1-\beta^2}{\rho}\int_R^\infty \rho(r,z)\frac{\partial\Phi(r,z)}{\partial r} e^{\int_R^r p(r'',z)\mathrm{d}r''}\,\mathrm{d}r, \tag{2.36}$$

$$\sigma_z^2(R,z) = \frac{1}{\rho}\int_z^\infty \rho(R,z')\frac{\partial\Phi(R,z')}{\partial z'} e^{\int_z^{z'} g(R,z'')\mathrm{d}z''}\,\mathrm{d}z', \tag{2.37}$$

[4]We assumed that the mass distribution of a galaxy is known from other sources, therefore we can calculate also the gravitational potential.

where p and g are the following functions

$$p = \frac{1-k_\theta^*}{R} + \frac{\partial \kappa^*}{\partial z}, \tag{2.38}$$

$$g = \frac{\xi^*}{R} + \frac{\partial \xi^*}{\partial R}. \tag{2.39}$$

The integration should be done along the characteristic curves, which are found when solving the following equations numerically

$$\frac{\mathrm{d}z}{\mathrm{d}R} = \kappa^*, \quad \frac{\mathrm{d}R}{\mathrm{d}z} = \xi^*. \tag{2.40}$$

The first/second equation describes the characteristic line for the first/second Jeans equation.

In principle, if we know free parameters a_2, b_2 and z_0, we can use either one of the Jeans equations to calculate all the kinematical characteristics of a galaxy component – one velocity dispersion component from the Jeans equation and other components according to the Kuzmin third integral. The overall result must not depend our use of either the first or the second Jeans equation and in principle we do not need both of them. Unfortunately, we do not know the free parameters and thus we need a way to constrain them. We use the above-mentioned condition that for the correct set of free parameters the Jeans equations must give the same velocity dispersions: we calculate the radial velocity dispersion (σ_R^2) from the first Jeans equation and the vertical velocity dispersion (σ_z^2) from the second one. Using the shape of the velocity ellipsoid (k_z^*) that was used in the Jeans equations, we can check whether the dispersions are consistent

$$\sigma_R^2 = \sigma_z^2 / k_z^*. \tag{2.41}$$

This equation (or an equivalent equation $k_z = k_z^*$) turns into identity only if both the Jeans equations and the third integral of motion are simultaneously satisfied, therefore we have a way to find the free parameters. It is implemented by cost function

$$\chi^2 = \int_0^\infty \int_0^\infty \left[\sigma_z(R,z) - \sigma_R(R,z)/\sqrt{k_z^*}\right]^2 \mathrm{d}R\mathrm{d}z \tag{2.42}$$

minimisation. Alternatively, more elaborate matching techniques can be used.

Once we have the value of either σ_R^2 or σ_z^2, we can calculate other dispersion components by the third integral approximation. The formula for σ_R^2 based kinematics are $\sigma_z^2 = k_z^* \sigma_R^2$, $\sigma_\theta^2 = k_\theta^* \sigma_R^2$ and the σ_z^2 based kinematics: $\sigma_R^2 = \sigma_z^2 / k_z^*$,

$\sigma_\theta^2 = \sigma_z^2 k_\theta^*/k_z^*$. The tilt of the ellipsoid comes from Eq. (2.5). In elliptical coordinates velocity ellipsoid parameters can be found with the following equations:

$$\sigma_1^2 = \frac{\sigma_z^2 \sin^2\alpha - \sigma_R^2 \cos^2\alpha}{\sin^2\alpha - \cos^2\alpha}, \tag{2.43}$$

$$\sigma_2^2 = \frac{\sigma_R^2 \sin^2\alpha - \sigma_z^2 \cos^2\alpha}{\sin^2\alpha - \cos^2\alpha}. \tag{2.44}$$

In case of $\alpha = 45^\circ$, there is 0/0 indetermination and the non-tilted ellipsoid parameters can be found using the dispersion ratio k_{12}.

An example of a model calculations of how well the consistency can be fitted and the statistical errors for each parameter can be seen in Sect. 5.1.1, where this model is applied to the Andromeda galaxy.

CHAPTER 3
FROM DYNAMICAL MODEL TO MEASURED KINEMATICS

In the previous chapter we described how to calculate the internal kinematics in each galactic point. The results of calculations must be naturally compared with observations, and for that we need to consider all observational effects. The aim of this chapter is to take into account the effects that change observed kinematics: galactic transparency, over the line of sight integration, the atmospheric smearing of image (seeing), possible changes due to observing instruments and differences due to spectral line fitting methods.

3.1 Line of sight effects in external galaxies

Galaxies are mostly transparent (or semi-transparent, in case of a dusty galaxy), dictating that we must take into account all the points on the line of sight. In the case of thin discs, galactic plane dominates in light budget when compared to regions above/below the galactic plane. All the most important parameters for us (e.g. stellar rotation velocity or a velocity dispersion) are proportional to brightness, hence, the galactic plane gives the highest contribution there. Thus, in the first approximation there is a possibility to calculate these parameters only in galactic plane (see Zhao et al. (2006) or an example), but some caution is needed here. Flatness and inclination angle of a galaxy are degenerated and the thinness assumption may not be fulfilled. In a general thick disc case, a more subtle approach is needed.

All observed images of external galaxies are projected to the plane of the sky. To make our model correspond to observations at each image point (X, Y), we must integrate our important parameters over the line of sight. We construct a coordinate set in a way that X and Y correspond to the apparent major and minor axis of the galaxy, respectively. An illustration of the coordinate set is given in Figure 3.1.

3.1.1 Integration of functions over the line of sight

Let f be a function to be integrated (e.g. luminosity density) and F denote resulting integrated over the line-of-sight value (e.g. luminosity surface density). Mathematically, there are three ways to implement the integration over the line of sight: integration over R, over z and over the isodensity ellipsoid major axis a for a specific density distribution. These implementations are equivalent, the differences only slightly affecting the accuracy and speed of the calculations.

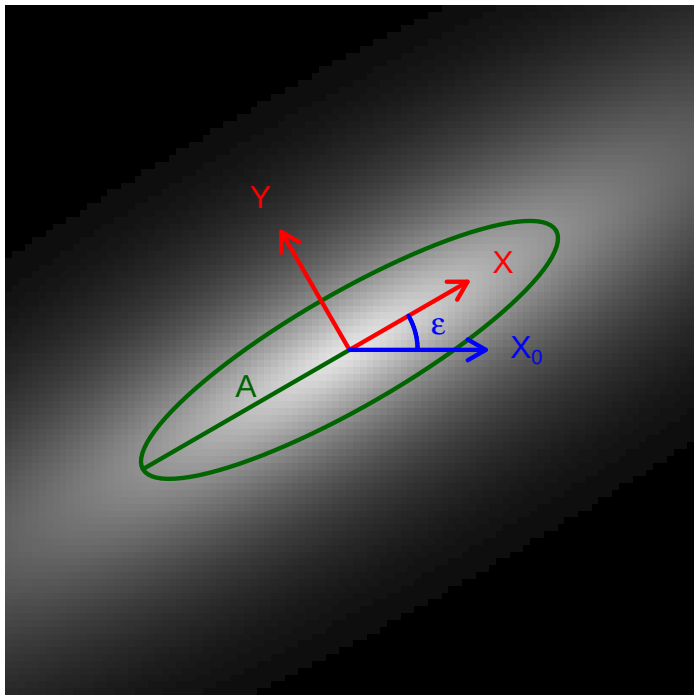

Figure 3.1: This figure illustrates the coordinate set for a model galaxy component. The centre of the coordinates coincides with the galaxy centre. X_0 denotes the horizontal axis of the image, X, Y are the major and minor axis directions on the plane of sky, ϵ is the position angle of the galaxy, A is the major axis length of the isophote.

Integration over a has an advantage when a is related to R and z in a simple way: $a^2 = R^2 + (z/q)^2$, i.e. there is an axial symmetry and the isophotes in R-z plane are ellipses. An advantage of integration over a is the ability to calculate F on the entire ellipse (in the $X - Y$ plane) with one integral, giving a huge advantage in computational speed. Disadvantages include the inability to integrate projected variables (e.g. velocity vector) and to take into account the influence of the dust along the line of sight. The formulae to integrate over a are as follows:

$$F(A) = 2\frac{q}{Q}\int_A^\infty \frac{f(a)a}{(a^2 - A^2)^{1/2}}\mathrm{d}a, \tag{3.1}$$

$$A^2 = X^2 + Y^2/Q^2, \tag{3.2}$$

$$Q^2 = \cos^2\gamma + q^2\sin^2\gamma, \tag{3.3}$$

where A and Q are the apparent major axis and axis ratio of isophotes on the model image on $X - Y$ plane, q is the intrinsic axis ratio of the galactic component, and γ is the inclination angle of the galaxy.

The other methods for integrating over the line of sight are implemented as integration over z and R. The advantage of these methods comes forth in nearly edge-on and face-on galaxies where inclination related functions (e.g. $1/\cos\gamma$) can have very

high or low values. Therefore during the integration, one should pay attention to convergence and accuracy, and choose the implementation formula accordingly. The formulae for integrating over z are:

$$F(X,Y) = \int_{-\infty}^{\infty} \frac{f(R(z),z)}{\cos\gamma}\mathrm{d}z, \tag{3.4}$$

$$R^2 = X^2 + \left(\frac{Y}{\cos\gamma} - z\tan\gamma\right)^2. \tag{3.5}$$

Integration over R can be calculated with the following equations:

$$F(X,Y) = \int_{X}^{\infty} \frac{f(R,z_1)+f(R,z_2)}{\sin\gamma\sqrt{R^2-X^2}} R\,\mathrm{d}R, \tag{3.6}$$

$$z_{1,2} = \frac{Y}{\sin\gamma} \pm \frac{\cos\gamma}{\sin\gamma}\sqrt{R^2-X^2}. \tag{3.7}$$

All the formulae given in this section describe a galaxy component. For corresponding parameter describing a whole galaxy, the integrated component parameters must be summed with weights proportional to the luminosities of components.

3.1.2 Integrating kinematic quantities over the line of sight

When we are interested in the kinematical properties of a component (observed line of sight rotational velocity and the velocity dispersion along the line of sight), the procedure is three-fold: we must project the internal motions to the line of sight direction, construct a velocity profile based on it, and integrate it over the line of sight.

The first part is the projection of the velocity vector and velocity ellipsoid tensor to the line of sight direction. These quantities are calculated from the Jeans equations: rotation velocities and velocity dispersions in the R (or z) direction with the shape parameters of the velocity ellipsoid, see Eqs. (2.37, 2.36).

For the rotational velocity, the projecting formula is simple:

$$V_{\mathrm{los}} = V_\theta \frac{X}{R}\cos\gamma. \tag{3.8}$$

For the velocity dispersions, the most intuitive method is to find the dispersions in the elliptical coordinate directions[1], and project the dispersion value according to

[1]For a gas component, no coordinate rotation is needed since velocity ellipsoid is isotropic.

the velocity ellipsoid orientation α and the line of sight angle. The formulae for the projection of the dispersions to the line of sight direction are:

$$\sigma_{\rm los}^2 = (\sigma_1^2 \cos^2 \alpha_{\rm L} + \sigma_2^2 \sin^2 \alpha_{\rm L}) \frac{R^2 - X^2 \sin^2 \delta}{R^2} + \sigma_\theta^2 \frac{X^2 \sin^2 \delta}{R^2}, \quad (3.9)$$

$$\alpha_{\rm L} = \left| \alpha - \arctan\left(\frac{R}{\tan \delta \sqrt{R^2 - X^2}} \right) \right|. \quad (3.10)$$

The second step is to construct velocity profiles at each point along the line of sight. This is a straightforward procedure as we assume velocity profiles to be Gaussians with parameters $V_{\rm los}$ and $\sigma_{\rm los}$. In the third step we must integrate the derived Gaussian profiles $\mathcal{G}(\dots)$ along the line of sight.

In the third step two different scenarios must be distinguished: gas kinematics (emission lines) and stellar kinematics (mostly absorption lines). In case of emission lines an additional particle is needed for collisional excitation of an atom or a molecule, therefore, the intensities of spectral lines must be proportional to the square of particle densities, meaning that when integrating along the line of sight in formulae (3.1, 3.4, 3.6) the integrand f must be proportional to squared density, instead of density[2]. In case of absorption lines each small line is created inside an individual stellar atmosphere, therefore, integrand is proportional to the number of stars or in case of single stellar population to the luminosity density $l = \rho/\Upsilon$. From here and onward, we assume that stellar kinematics is studied and use l for weighting.

Comparison of the model calculations with observations is best done when the comparable are calculated as similarly as possible. One possibility is to compare each velocity $f = \rho V_{\rm los}$ or velocity dispersion $f = \rho \sigma_{\rm los}^2$ (ρ is the weight in f) from model and observations, but they are affected by systematics of forming spectral lines in external galaxies. In the ideal case we do not calculate an intermediate result (mean and standard deviation of the velocity profile), but compare spectral lines directly with the model velocity profile. This can be done by allowing integrand to stay dependent on velocity (or equivalently wavelength in case of observed spectral line) and therefore compare the velocity profile with an observational data-cube:

$$I(X, Y, v) = \int_{\rm los} l^s(R, z) \mathcal{G}(v, V_{\rm los}, \sigma_{\rm los}), \quad (3.11)$$

where $\mathcal{G}$ is assumed to be Gaussian distribution in each line of sight point, I is the resulting velocity profile, and s corresponds to the nature of the component: one in case of stellar modelling, and one or two in case of gas, depending whether the

[2] An exception is when the excitation is caused by stellar radiation, in which case the weight should be proportional to gas density

excitation originates from light intensity or from collisions of gas molecules. It is important to point the attention of the reader, that resulting integrated velocity profile $I(X, Y, v)$ is not Gaussian anymore. In case of Schwarzschild modelling, it can be taken into account more directly (Cretton et al. 1999).

Another approach to calculate line of sight integrated kinematics is to weigh. To calculate the observed velocities, calculated velocities at each point along line of sight are weighed by the luminosity at that point as it was done by Tempel & Tenjes (2006) and Binney & Tremaine (2008). Analogously dispersions can be calculated. However, in this method there is a concern it does not take into account the possible increase of velocity dispersions when velocity peaks are situated side-by-side in the recessional velocity space.

3.1.3 Integration over the line of sight in presence of dust

Observations indicate that there may be a substantial amount of dust in disc galaxies. Thus, it is necessary to study and if needed to include dust attenuation to model quantities (this is equivalent to removal of the dust effect from observed quantities). For this we must weigh each point in the line of sight with the inverse attenuation where the light has yet to travel. The latter quantity can be characterised with $e^{-\tau}$, where τ is the optical depth and can be found by integrating the attenuation coefficient $\tau = \int_{\mathrm{los}} \kappa_{\mathrm{d}}$ along the remaining part of the line of sight. If we can assume that dust has uniform properties and dust-to-gas ratio is constant, we can tie the gas density and the attenuation coefficient of dust distribution with $\kappa_{\mathrm{d}} = n\nu = \rho_{\mathrm{gas}} m_0^{-1} \nu_{\mathrm{d}}$, where n is number density of atoms, ν_{d} the cross-section of dust molecule, ρ_{gas} gas density, and m_0 the average mass of a gas molecule. Thus we have the means to tie attenuation with the gas density profile.

The integration over the line of sight is done with the following formula (with an assumption we are located at $+\infty$):

$$F_{\mathrm{d}}(X, Y) = \int_{-\infty}^{\infty} \frac{e^{-\tau(X,Y,z)} f(R(z), z)}{\cos\gamma} \mathrm{d}z, \tag{3.12}$$

$$\tau(X, Y, z) = \int_{z}^{\infty} \frac{\kappa_d(R(z'), z')}{\cos\gamma} \mathrm{d}z', \tag{3.13}$$

where f again denotes a function to be integrated and being already weighed by luminosity and F is the observed quantity. The use of this formula assumes the dominance of absorption when compared to scattering, which Bianchi (2007) showed to be valid.

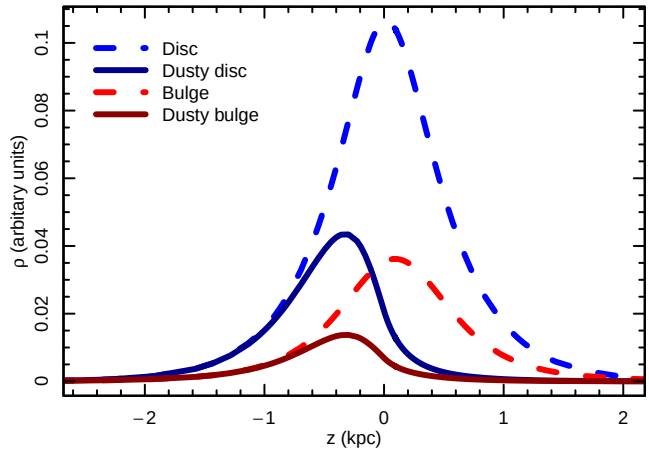

Figure 3.2: The contribution of different regions to the over the line of sight integrated luminosity as a function of z coordinate. One can see that when the dust attenuation is taken into account, the origin of most of the luminosity shifts toward the viewer. In addition, the kinematic properties of these regions are different, hence a change in the observed velocity distribution is induced. The position of the line of sight is $X = 3.6$ kpc and $Y = 0.1$ kpc of a M31-like galaxy (see Sect. 5.1).

The absorption by dust modifies the observed quantities: at more distant points along the line of sight the dust attenuation effect is higher and these points give smaller contribution in F. As a result, the effective origin of function to be integrated will be shifted toward the viewer as is seen from Figure 3.2.

3.2 Additional kinematic effects inside external galaxies

There are some additional effects due to the inner structure of galaxies that cannot be described within an axisymmetric model. In this section we bring them forth and estimate, how much error they would introduce if we neglect them.

Most galaxies contain at least some form of non-axisymmetric substructures like bar, spirals, stellar streams etc, each of them able to influence the observed kinematical properties of a galaxy. Mostly, these substructures do not create a bulk motion but increase the chaotic component, which is described by velocity dispersions. Unfortunately, the amplitude of the dispersions increase cannot be uniquely determined, as the dispersions increase is a function of time and the effect is cumulative, as it was shown in simulations by Minchev & Quillen (2006). One aspect is the elevated level of dispersions, another is the distorted shape of the velocity dispersion ellipsoid: the axial ratio on the dispersion ellipsoid in the plane of a galaxy may decrease from

0.6...0.9 outside of spirals, to 0.25...0.5 in the convex edge of the spiral (Vorobyov & Theis 2008). Also, the gas motions are influenced by the presence of a bar especially in the outer regions of bar (Fujimoto et al. 2014).

Even in galaxies with no clear spirals and a bar, the observed velocity dispersion may have a tendency to be larger compared to model ones. It comes from the fact that a significant part of stars are binary or multiple stars. As stars are formed, they form in molecular clouds and in the form of an open cluster. From there they dissolve over a long time. When a modelled galaxy has a high star formation rate, substantial fraction of stars are still inside open clusters increasing the dispersions by $\gtrsim 10$ km s^{-1}. Additionally, as the stars are binaries, their orbital motion also increases dispersions. In case of globular clusters Bianchini et al. (2016) estimated this bias to be $0.1 \ldots 0.3$ km s^{-1}.

One source of elevated rate of dispersion is the active galactic nucleus, where gas clouds may have velocity dispersions in the order of 1000 km s^{-1}. Luckily, they are easily recognised and appropriate steps can be taken.

The cumulative effect of various effects of the velocity dispersion is taken into account by adding corresponding dispersions

$$\sigma_{\mathrm{total}} = \sqrt{\sigma^2_{\mathrm{galaxy}} + \sigma^2_{\mathrm{open\ clusters}} + \sigma^2_{\mathrm{bar,spirals}} + \sigma^2_{\mathrm{other}}}. \tag{3.14}$$

As the squares are summed, smaller contributions are greatly suppressed, which means that non-axisymmetric substructures may give higher contribution when the contribution from galactic regular potential is smaller i.e. above/below the galaxy plane. Luckily, in these regions there are few structures seen as a rule.

3.3 Distortions of kinematics in atmosphere and instrumentation

To make modelled quantities as comparable to observations as possible, we must mimic the journey of light from a galaxy to the telescope. The regions, where light was, can be divided into four groups: in external galaxy (covered in the last two sections), intergalactic medium (where redshift to light is produced), Milky Way, and on Earth. In the intergalactic medium, only expansion-related changes are produced to spectral line, which are reversed during redshift correction, and therefore are not discussed here.

The attenuation in our Galaxy can be calculated using infrared dust maps from Schlegel et al. (1998). For kinematics, this does not create any discrepancies. The next steps (atmospheric smearing – seeing, the convolution due to the spectrograph slit, CCD inhomogenities and the exact mechanism to extract kinematics from observed spectra) do change kinematic data, thus these will be considered more throughly in the next sections.

3.3.1 Distortions due to seeing and slit width of a spectrograph

Seeing is an atmospheric effect that causes the high resolution light distribution to be smeared and is caused by small-scale turbulences in higher atmosphere. In case where the size of the observed galaxy is comparable to the seeing (usually $0.5 \ldots 2''$depending on astroclimate) it is essential to take seeing into account. Mathematically, it consist of convolving model image with a function describing seeing, being usually approximated with a normal distribution:

$$I_{\mathrm{seeing}}(X, Y, v) = \int_{-\infty}^{\infty}\int_{-\infty}^{\infty} I(X', Y', v)\mathcal{G}(r, \sigma_{\mathrm{seeing}})\mathrm{d}X'\mathrm{d}Y', \quad (3.15)$$

$$\mathcal{G}(r, \sigma_{\mathrm{seeing}}) = \frac{1}{\sqrt{2\pi\sigma^2_{\mathrm{seeing}}}} \exp\left(-\frac{r^2}{2\sigma^2_{\mathrm{seeing}}}\right), \quad (3.16)$$

$$r = \arctan\left[\sqrt{(X - X')^2 + (Y - Y')^2}/d_A\right], \quad (3.17)$$

where d_A is angular distance[3] of the galaxy, $\mathcal{G}$ is zero-mean Gaussian distribution, σ_{seeing} is standard deviation of the seeing profile measured in arcseconds[4] and X, Y are distances in image plane along the major and the minor axis in physical units. To increase the accuracy even more, the seeing must be replaced with the convolution of seeing and point spread function (or just with the point spread function if the telescope uses adaptive optics). Quite often, the Gaussian profile is sufficient to describe the combined effect of seeing and point spread function. In very nearby galaxies, such as Andromeda galaxy (M31), the seeing has a rather little effect, so it can be neglected.

A Similar effect of smearing can be seen in reconstructing the slit into a model image. The difference is the shape of convolution function, being a box function rotated according to the position angle of slit. Sometimes, especially when observing dim distant galaxies, a wide slit is used in order to reduce the exposure time. This increases the need take into account the smearing due to slit during modelling. The effect of both seeing and slit can be seen in Figure 3.3.

In addition, when the slit of the spectrograph is not aligned with the major axis of a galaxy, the dust can cause some additional distortions to observations. A more thorough description is given in Sect. 6.1.

[3]The angular distance relates to Mattig and luminosity distance by being (1+redshift) and (1+redshift)^2 times smaller.

[4]It is common to measure seeing as full width at half maximum, which is $2\sqrt{2\ln 2} \simeq 2.355$ times larger than the standard deviation of Gaussian distribution.

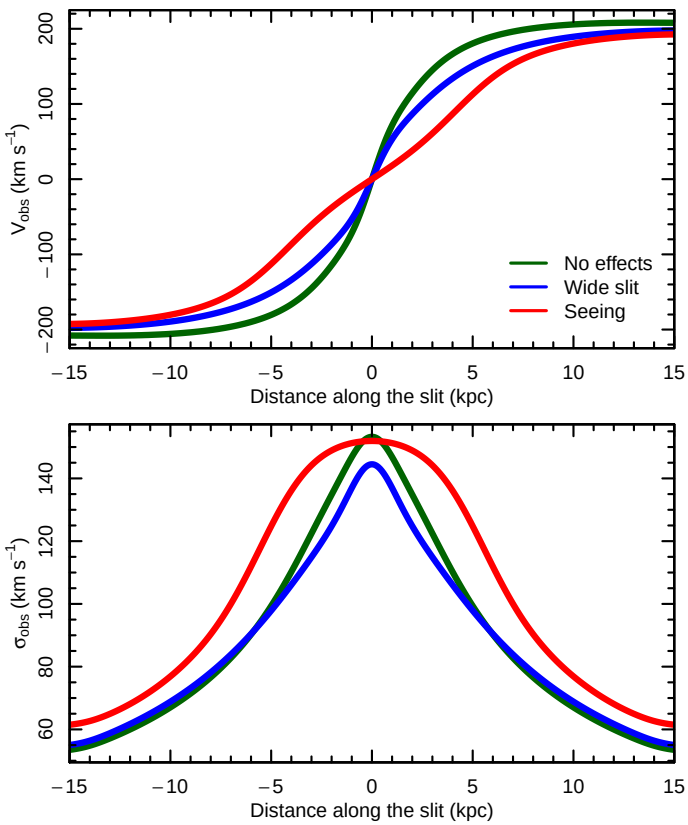

Figure 3.3: The effect of atmospheric seeing and the width of spectrograph slit to the kinematics of the Andromeda galaxy mimicked to be at the distance of 2000 Mpc with seeing $1''$ and spectrograph slit width $1''$. Different lines indicate how much influence they have on measured rotation curve and dispersion distribution. The seeing influences the kinematics more than slit width, mostly in the central part.

3.3.2 Extracting kinematics from spectroscopic data

For elliptical galaxies and bulges of disc galaxies a common way to describe the line of sight stellar motion is Gauss-Hermite polynomials, which are defined as

$$I(v) = \frac{e^{-y^2/2}}{\sigma\sqrt{2\pi}}\left[1 + \sum_{m=3}^{4} h_m H_m(y)\right], \tag{3.18}$$

$$y = \frac{v - v_0}{\sigma}, \tag{3.19}$$

where H_m are Hermite polynomials, v_0 and σ are mean and standard deviation of velocities in normal distribution, h_3 and h_4 are parameters describing non-Gaussianity of spectral lines. Gaussian distribution is a special case of Gauss-Hermite polynomials, where $h_{i>2} = 0$. Fitting of the velocity distributions with Gauss-Hermite polynomials is a good way to include extra freedom in shapes of spectral lines, but it also has small drawbacks. Firstly, some parts of the distribution function can be negative, which is unphysical when considering velocity distribution. The second disadvantage is a minor correlation between v_0–h_3 and σ–h_4 (Cappellari & Emsellem 2004), which could introduce considerable errors when fitting model parameters to measured ones. It can be solved in some degree by first fitting with a Gaussian profile and thereafter determining h_3, h_4 parameters with fixed v_0 and σ. Another source of error is low sampling in spectral space: the whole spectral line shape is sometimes binned to a few pixels on CCD, especially in case of distant galaxies, where dimness of galaxy is often compensated by lowering the spectral resolution.

As galaxy spectrum is crowded by absorption lines, it is often difficult to separate individual lines and to determine their widths. Therefore, two different families of techniques have been developed: the Fourier deconvolution method (see e.g. Bender 1990) and fitting the maximum of correlation function between observed and template spectra. Some methods try to consider the line of sight velocity more directly (Rix & White 1992). Convolving the line of sight velocity distribution with template spectra and removing low-frequency noise by fitting polynomial is another approach to model spectra (Cappellari & Emsellem 2004). There are analogus methods to find emission and absorption kinematics together (Sarzi et al. 2006).

These methods no not take into account that line of sight velocity distribution may depend on wavelength. Dust in external galaxies and different bulge-to-disc luminosity ratios can create such an effect (see Sect. 6.1), making it more difficult to model the line of sight velocity distribution directly.

Emission lines caused by the gas are usually seen as quite distinct emission lines, making it possible to fit these lines directly (Weiner et al. 2006). Certainly, more accurate result can be found by fitting several lines together, usually Hβ, O[III] and O[II] lines.

CHAPTER 4
DENSITY DISTRIBUTION ESTIMATION

In order to apply the dynamical modelling to a galaxy, we first need to know the density distribution of the galaxy. We describe a galaxy as a sum of different components. Usually four components are used: stellar bulge, stellar disc, gas disc and dark matter halo. In this chapter, we explain how to model the mass distribution of luminous components by using the photometric data.

There are two main approaches to model the luminosity distribution of a galaxy: the first approach is to use superposition of many simple luminosity distribution profiles, and the second one is to use a small number of well-chosen profiles to mimic the light distribution of a galaxy. For the first approach, the most wide-spread technique is multi-Gaussian expansion (see Cappellari et al. (2002) for an excellent use of it). It has an advantage that a simple analytical formula for gravitational potential exist, allowing to calculate kinematical descriptive functions of a galaxy fast. The disadvantage, however, is that individual components are not physical and thus interpretation of calculated results is difficult. A more common approach is to fit the light distribution of a galaxy with a few well-chosen density profiles, so-called designer basis functions.

In the equations for dynamic calculations there is a spatial (three-dimensional) density distribution. Thus, another issue will arise if one wishes to fit the photometrical observations of a galaxy with a surface density law and deproject it, or to fit a 3D profile directly. In the latter case, one needs to integrate spatial density over a line of sight in order to fit the observed image (see Sect. 3.1.1). Astronomers, who are interested in dynamic modelling (as we are), usually prefer to fit a 3D profile directly.

4.1 Modelling the density profiles

4.1.1 The procedure of photometrical modelling

The goal of photometrical modelling is to have a model image as similar as possible to the observed image. A quite common technique is to maximise the likelihood for each pixel belonging to a model with a certain parameter set. As the errors of observed luminosities usually include Gaussian noise, maximising the likelihood is equivalent to minimising the loss function defined as

$$\chi^2 = \sum_{X,Y \in \mathrm{mask}} \frac{[L_{\mathrm{model}}(X,Y) - L_{\mathrm{obs}}(X,Y)]^2}{s^2(X,Y)}, \tag{4.1}$$

where $L_{\rm obs}$ is the observed surface brightness in a pixel with coordinates (X, Y), $L_{\rm model}$ is a model luminosity surface density integrated over line of sight and s describes the error of the observed luminosity in each pixel. For the s value (see Howell 2006), there are a few sources: errors from readout noise of a CCD, flat field correction (in order to uniformise the sensitivity of CCD), data reduction (e.g. from dithering) and the Poisson noise. Usually an image does not contain only the observed galaxy, therefore sources not being a part of the galaxy should be masked out and excluded from χ^2 calculation. These masked out sources include foreground stars, other galaxies or parts of other galaxies and in some cases (e.g. if we are interested mainly in mass distribution) also the regions that give high contribution to luminosity, but have very little mass. These are the regions with high star formation rate like clumps in high redshift galaxies and spirals.

Using in modelling surface photometry observations done with different filters may produce different parameter sets for a galaxy (Vulcani et al. 2014). This is not surprising as in different filters relative contribution of components in overall luminosity distribution may be different: in red filter, which describes the distribution of intermediate and lower mass stars, the overall mass distribution the total profile is inclined to be more bulge-dominated while in blue or ultraviolet filters describing younger stars, the total profile reminds more a disc-dominated galaxy. Analogously, disc parameters, especially thickness, may be different in different filters as star formation is taking place near the gas rich plane, making parts at low altitudes of discs bluer while the old stellar population dominate at higher altitudes. Thus, discs seem thicker in red filter. The solution is to use a larger number of components when the difference of component sizes is seen in different filters. In cases when residuals images in different filters differ systematically (e.g. if arcs appear in some residual images), the number of components in total fitted profiles should be increased. Mostly a two-component (bulge + disc) is sufficient, in which case all the parameters, except luminosity, are fixed per component for all the filters.

After having constructed the correct χ^2 expression, it needs to be minimised. Finding the global minimum can be sometimes tricky, especially if there are many free parameters. We decided to use multinest (Feroz & Hobson 2008; Feroz et al. 2009, 2013) + simplex from Numerical Recipes (Press et al. 1992). Multinest has bayesian approach that allows to sample large parameter space and specify the most probable region in parameter space. Simplex is good for finding local minima by iteratively moving along the gradient of χ^2. Using purely simplex can give local minima instead of global one, therefore it is best to use them in combination.

4.1.2 The Einasto profile

For practical applications, one has to choose an analytic form for the density distribution profile. Picking one that describes a realistic galaxy well can be difficult. The aim is to choose a profile form that can fit the observed luminosity distributions, while being simple enough with a small number of free parameters and with accurate formula for the gravitational potential. This is not an easy task, but it seems that all the necessary conditions are satisfied by the Einasto profile (Einasto 1969):

$$\rho(a) = \rho_c \exp\left\{-d_N\left[\left(\frac{a}{a_c}\right)^{1/N} - 1\right]\right\}, \tag{4.2}$$

with an equivalent form of

$$\rho(a) = \rho_0 \exp\left[-\left(\frac{a}{ka_0}\right)^{1/N}\right]. \tag{4.3}$$

The parameters in the Einasto profile are as follows: N describes overall shape, a_c or a_0 is a scale length describing the size of a galaxy, d_N and k are normalising parameters to have a_c and a_0 their physical meaning (a_c contains half of the total mass and a_0 is the harmonic mean radius), ρ_c is the density at a_c and ρ_0 is the central density. The total mass of the component can be found with

$$M = \frac{4\pi q a_0^3 \rho_0}{h}. \tag{4.4}$$

Values of h and k depend on N and can be found from formulae

$$k = \frac{\Gamma(2N)}{\Gamma(3N)}, \quad h = \frac{\Gamma^2(3N)}{N\Gamma^3(2N)}, \tag{4.5}$$

where Γ is a Gamma function. For more details and calculation of d_N see appendix B in Tamm et al. (2012). In the present work we use an empirical approximation $d_N = 3N - 0.333 + 0.0079/N$.

A similar and more widely used function to describe the surface density distribution of a galaxy is Sérsic profile. The main difference between the Einasto and Sérsic profiles is their dimensionality: Einasto profile describes spatial density distributions while the Sérsic profile surface density distributions. There have been attempts to unify both profiles but with no general results (Dhar & Williams 2010). The integrated over the line of sight density distribution (4.3) is close, but not identical to the Sérsic law (Sersic 1968) for surface densities (see Tamm & Tenjes 2006, for an illustrative comparison). Dhar & Williams (2010) also concluded that for some N

values, the surface density profile from over the line of sight integration of Einasto profile can be analytical.

Another standard quantity needed for modelling the galaxy dynamics, is the expression for gravitational potential, or derivative of the potential in case of the Jeans modelling. The gravitational potential derivatives for an inhomogeneous ellipsoidal mass distribution can be expressed in a convenient form (see Tenjes et al. 2001)

$$\frac{\partial\Phi(R,z)}{\partial R} = R\frac{GMh}{(ea_0)^3}\int\limits_0^{\arcsin(e)}\rho^*(a')\sin^2 x\,\mathrm{d}x, \tag{4.6}$$

$$\frac{\partial\Phi(R,z)}{\partial z} = z\frac{GMh}{(ea_0)^3}\int\limits_0^{\arcsin(e)}\rho^*(a')\tan^2 x\,\mathrm{d}x, \tag{4.7}$$

where $a' = \frac{\sin^2 x}{e^2}\left(R^2 + \frac{z^2}{\cos^2 x}\right)$, $e = \sqrt{1-q^2}$ is eccentricity and ρ^* is an exponential part of the density law (4.3), and G is the gravitational constant. For isotropic density distribution, the formulae are

$$\frac{\partial\Phi(R,z)}{\partial R} = R\frac{GMh}{a_0^3}\int\limits_0^{1}\rho^*(a')u^2\,\mathrm{d}x, \tag{4.8}$$

$$\frac{\partial\Phi(R,z)}{\partial z} = z\frac{GMh}{a_0^3}\int\limits_0^{1}\rho^*(a')u^2\,\mathrm{d}x, \tag{4.9}$$

where $a'^2 = u^2(R^2+z^2)$.

4.2 Reliability of the parameters of photometric model

To have a reliable model for the density of the stellar components, one needs know the robustness of the output parameters. In order to investigate it, we constructed model images that mimicked the observing conditions and modelled these galaxies. We denote these constructed galaxies as test-galaxies.

4.2.1 Test-galaxies for estimating robustness of photometric model

The robustness of an estimate is most practical, when the model galaxies resemble the observed galaxies, i.e. have realistic parameters. Therefore, we started from SDSS (York et al. 2000) galaxies. We chose 1000 galaxies with maximally uniform distribution on the main characteristics: luminosities, luminosity profiles, sizes, axial

rations, bulge-to-disc ratios and inclination angles. Galaxies were assumed to consist of the bulge and the disc. Elliptical galaxies were described in the same way, but with rather high bulge-to-disc ratios.

The process of creating test-galaxies was a straightforward one: we selected a model from the SDSS sample, convolved it with a point-spread function from the SDSS database, added a Poisson noise to each pixel according to its luminosity, and inserted the image to an empty background field. The latter contains all the possible noise from the instrumentation. An example of the created test-galaxies can be seen in Figure 4.1.

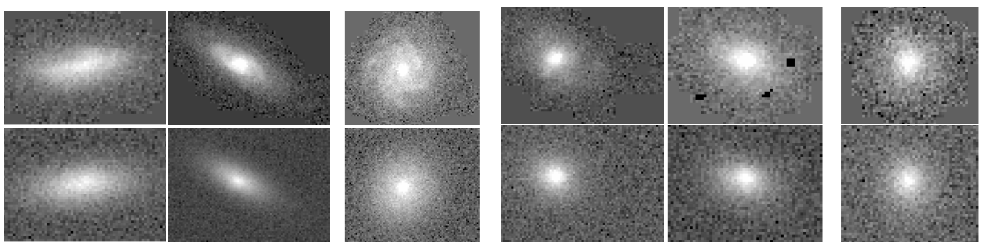

Figure 4.1: Example of the test-galaxies. The top row shows the observed galaxies that test-galaxies are based on, and the bottom row the test-galaxies themselves.

The subsequent re-modelling was done by minimising the sum of χ^2 in each filter according to Eq. (4.1) with Multinest and simplex minimising algorithms. The modelling parameters (number of components, choice of the profiles etc) of the re-modelled galaxies were the same as they were for creating of the test-galaxies.

4.2.2 The reliability of the photometric model parameters

Once we have re-modelled the test galaxies, we are able to compare derived parameters with the original ones i.e. to test our modelling process. First, we are interested in seeing how well the overall light distribution of a galaxy is restored. This is shown in Figure 4.2. The intensity at each a value was found by fitting a thin ellipse to the model isophotes. It is seen that in the inner parts of galaxies modelling accuracy stays within 5%, the outer parts fits diverge more. A probable reason for the latter is that the outer regions are suffering from noise dominance: as the luminosity drops, the absolute difference between the intrinsic and restored light distributions is dominated by random noise, not due to luminosity differences, and therefore it has lower accuracy. There are no systematic differences at any radius.

From the kinematical point of view the bulge and disc are very different components: the bulge is dominated by random motions while disc is dominated by rotation. When studying kinematics it is important to know the relative contribution of these

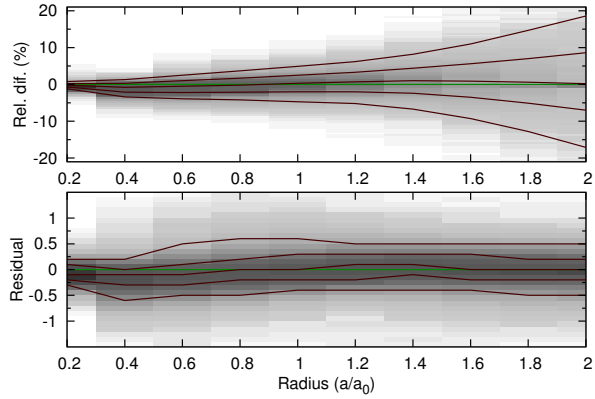

Figure 4.2: This figure contains information on how well the overall luminosity distribution was recovered during the test-galaxy modelling. The top figure shows the relative difference between the modelled and true value, having lower values in the central region. The bottom figure shows the absolute, the top one the relative difference between the true and modelled value. The dark red lines show the 0.1, 0.25, 0.5, 0.75, 0.9 quantiles of the distribution on each radius.

components in overall kinematics. We derived that the total luminosity of a component can be restored with the accuracy of 0.1^{m} (in 50% of cases) and 0.2^{m} (in 90% of cases). These numbers are nearly independent of the actual luminosity. Thus, in case of equally bright bulge and disc, the resulting bulge-to-disc ratio can be restored with approximately $25 \ldots 50\%$ accuracy (the 0.5 and 0.9 quantile), see Figure 4.3. When one of the components is dominating, there remains too little information to recover the luminosity of the other component and the corresponding accuracy is poor. From the kinematical point of view, the smaller component contributes little to the potential, making the error due to bulge-to-disc ratio less severe.

The inclination angle of a galaxy and thickness of a component are the parameters influencing galaxy kinematics significantly. As we can see from the Eq. (3.3) describes the observed axial ratio of an isophote, the inclination angle of a galaxy and the intrinsic thickness of a component are mutually related and thus their determination is a degenerated problem. Figure 4.4 shows how well the restoration of the inclination angle of a galaxy can be done. In case of bulge-dominated galaxies, the inclination is restored with $10 \ldots 20^{\circ}$ accuracy. Although the error is enormous, this influences galaxy kinematic only moderately, since bulges are more or less spherical. For disc galaxies the restoration accuracy of the inclination angle is $\lesssim 5^{\circ}$, but the accuracy is decreasing as the orientation of a galaxy becomes more face-on. For pure discs the differences between true and modelled values are even $\lesssim 3^{\circ}$ and for purely

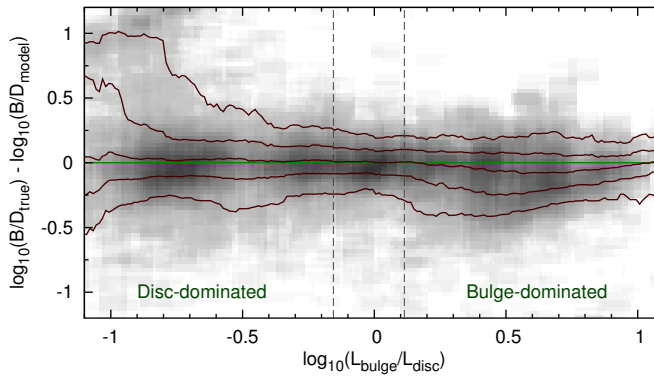

Figure 4.3: This figure shows the accuracy of restoration of the bulge-to-disc ratio. The best restoration is done when bulge and disc have similar luminosities, while it is somewhat worse is when one of the component dominates (see text for explanation). The dark red lines show the 0.1, 0.25, 0.5, 0.75, 0.9 quantiles.

elliptical galaxies they are $\gtrsim 20^{\circ}$. The other parameter that changes the observed ellipticity of isophotes is the intrinsic axis ratio of component (q). Figure 4.5 shows that in half of the cases, it can be restored by $\lesssim 0.05$ for disc, with a small systematic bias (overestimation) by the model. Unfortunately, for about 20% of the galaxies, the q is too uncertain to be useful, since it introduces too big errors in modelling the galaxy kinematics.

4.3 Adding the dark matter and the gas to the overall density distribution

As mentioned before, in addition of the stellar components a galaxy also contains gas and dark matter components. These components also need to be taken into account when modelling the dynamics of a galaxy.

The gas component is difficult to observe directly, as the gas may exist in different forms being not equally well observable. The amount of the atomic hydrogen can be calculated from 21cm line observations. The amount of molecular hydrogen can be calculated from CO observations and by knowing a corresponding conversion factor. Of course the amount of helium should be added. These methods contain some uncertainties, since the amount of neutral gas with higher temperatures is only poorly known and the correlation between the amounts of CO and H_2 is not known well enough either. But in any case, the gas distribution needs to be taken into account in models.

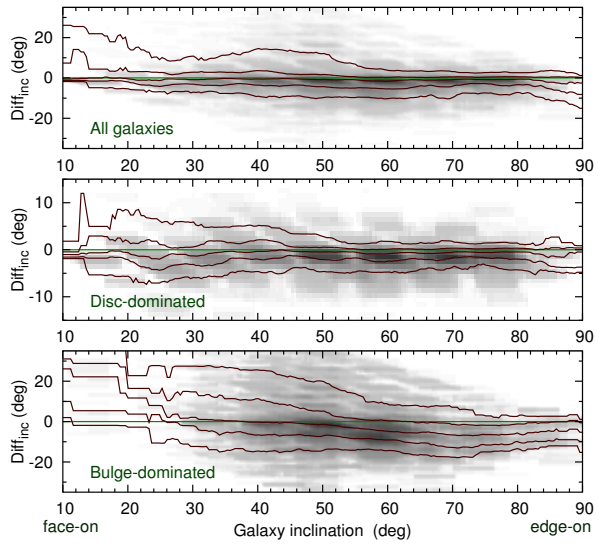

Figure 4.4: This figure illustrates how well the inclination angle of a galaxy can be restored. The top panel shows it for all galaxies, the middle for disc dominated galaxies, and the bottom one for bulge dominated galaxies. The dark red lines show the 0.1, 0.25, 0.5, 0.75, 0.9 quantiles.

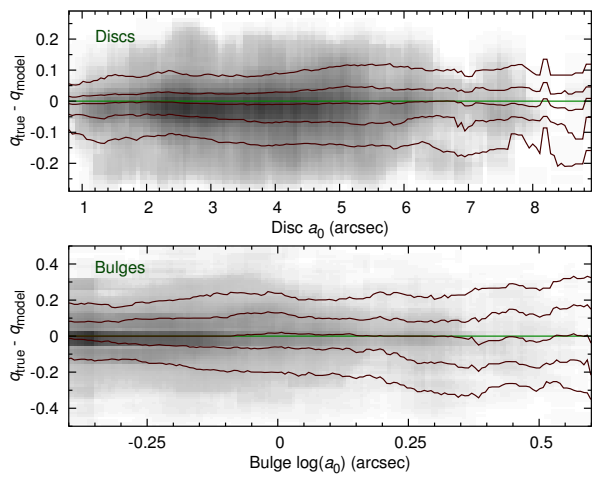

Figure 4.5: This figure illustrates how well the flatness of a galaxy component can be restored. The dark red lines show the 0.1, 0.25, 0.5, 0.75, 0.9 quantiles.

The dark matter halo is a component the mass distribution of which is the most uncertain. This component gives the highest contribution to the overall galaxy gravitational potential far from the centre and at these distances we can calculated its density distribution by using the rotation curve of a galaxy and the contribution of other components. Unfortunately quite often the extents of the rotation curves are limited and additional data are needed. For example, some constraints to the mass distribution of the dark halo can be derived by using the kinematics of globular cluster systems, the temperatures of hot X-ray emitting gas etc. Commonly, the rotation velocities of the gas, being quite close to the circular speeds (see Section 2.2) are used to constrain the dark matter halo mass distribution. The shape of the density profile is assumed to be the same as it results from the N-body simulations (see e.g.(Navarro et al. 2004)), giving the Einasto parameter $N = 6$.

To sum up, the dynamic modelling requires the overall density distribution. This density distribution can be derived by adding the densities of all the components: stellar bulge and disc, the gas disc and the dark matter halo. For stellar components, the density profiles can found from their luminosity distribution profiles by assuming a certain mass-to-light ratios or by fitting the observed spectral energy distributions to the model spectra and deriving the stellar mass. The gas and the dark matter density distributions were derived from the intensity distributions of some emission lines and from the kinematics of the gas component, respectively. As the gravitational potential and the mass density are additive quantities, the overall potential and density are found by simple summation.

CHAPTER 5
APPLYING THE MODEL TO OBSERVED GALAXIES

In this section we apply the dynamic models that were introduced in Chapter 2 on two datasets. The gas model is applied to moderately distant galaxies in order to find the intrinsic thickness of gas discs, and the stellar model on our neighbouring galaxy M31 for testing the model.

5.1 Applying the gas dynamic model

The purpose of this application of the gas dynamic model is to apply it on galaxies at redshift ~ 1 to find weather we can get robust model for these galaxies and be able to extract the thickness of the gas disc from these observations.

5.1.1 The data and assumptions for the dynamic model

We applied the gas dynamic model described in Section 2.2 to a sample of distant galaxy observations. We chose a sample of 27 galaxies in GOODS[1] North region, where both photometric and spectral observations have been done. The photometric observations were used to construct the density distribution needed for the gas model input. Kinematic data were used to compare the model results with and to constrain density distribution of components that were not included in the photometric model.

The photometric data originate from Hubble Space Telescope observations, which were observed in four filters (B, V, i and z) with ACS camera (Giavalisco et al. 2004). The spatial resolution of the dithered images was $0.03''$. As we needed the mass distribution, which is best described by the reddest filter image, only z filter data were used during the photometric modelling. The overall stellar mass was estimated from the spectral energy distribution with the MAGPHYS program (da Cunha et al. 2008) in which spectro-photometric modelling is applied. It is based on the public multi-wavelength catalog by Berta et al. (2011). This catalog includes point-spread function matched photometry in ACS B, V, i, z, FLAMINGOS J, H, K and IRAC 3.6, 4.5, 5.8, 8.0 micron, obtained with the ConvPhot code (Grazian et al. 2006). The output of the spectral energy distribution modelling were the stellar and dust masses. The gas mass that was needed in kinematic modelling was found from these, based on the relations from Walter et al. (2008) and Leroy et al. (2011).

[1] http://www.stsci.edu/science/goods/

The kinematic data used during the modelling were observed by Keck II telescope as a part of Team Keck Redshift Survey (TKRS) project (Wirth et al. 2004). The extraction of the rotation curve and velocity dispersion distribution of gas was done by Weiner et al. (2006). They used [O II] 3727 Å doublet spectral line and additional lines when available. During the observations, the seeing conditions were between $0.6 \ldots 1$" and the width of the spectrograph slit was 1". The slit was mostly aligned well with the major axis of the galaxy, with a few exceptions, and even then it remained smaller than $\sim 40^\circ$. As both the seeing and the width of the spectrograph slit are comparable with the size of a distant galaxy, neither of them can be ignored when calculating model kinematics.

5.1.2 Comparison of the model gas kinematics with observations

The assumptions about the galaxy that we modelled are axisymmetry and stationary (as kinematic model assumes), which we took into account when making the galaxy selection. We assume the galaxies consist of four components: stellar bulge, stellar disc, gas disc and the dark matter halo. The stellar component distribution parameters are found from photometric modelling. As we did not have information on the gas disc, except the mass, all of the gas disc parameters were free (a_0, N, q) and needed to be fitted during the kinematic modelling. The dark matter halo had also ρ_c and a_c as free parameters, but due to their degeneracy in inner parts of the galaxy, we kept a_c fixed at 100 kpc. Therefore we had four parameters to be modelled based on the kinematic data.

The first part of applying the model was to find the density distribution using the photometry of the galaxies. We fitted the over the line of sight integrated Einasto profile to observed z filter image. Mostly the photometric fitting gave adequate results, an example can be seen in Figure 5.1. The residual image contains only a non-axisymmetric substructure, which indicates that all the major components are included.

The quality of the parameters resulting from the dynamic model cannot be considered very accurate. Firstly, the observed kinematics had asymmetries in their rotation curve and dispersion distribution. Most probably they originate in the bright clumps of star formation, which has kinematics of its own (both internal and with respect to local frame) and high luminosity from young blue stars, making it the dominant part in spectrum. Since the bright regions have different kinematics than the galaxy, they cannot be included in the modelling, hence the amount of usable data was reduced. Fortunately, the bright spots do not influence much potential (due to low mass-to-light ratio), and therefore the applicability of the dynamical model. The second shortcoming of the application was high errors of velocity dispersions: as the gas disc has more influence on velocity dispersions than rotation curve, we

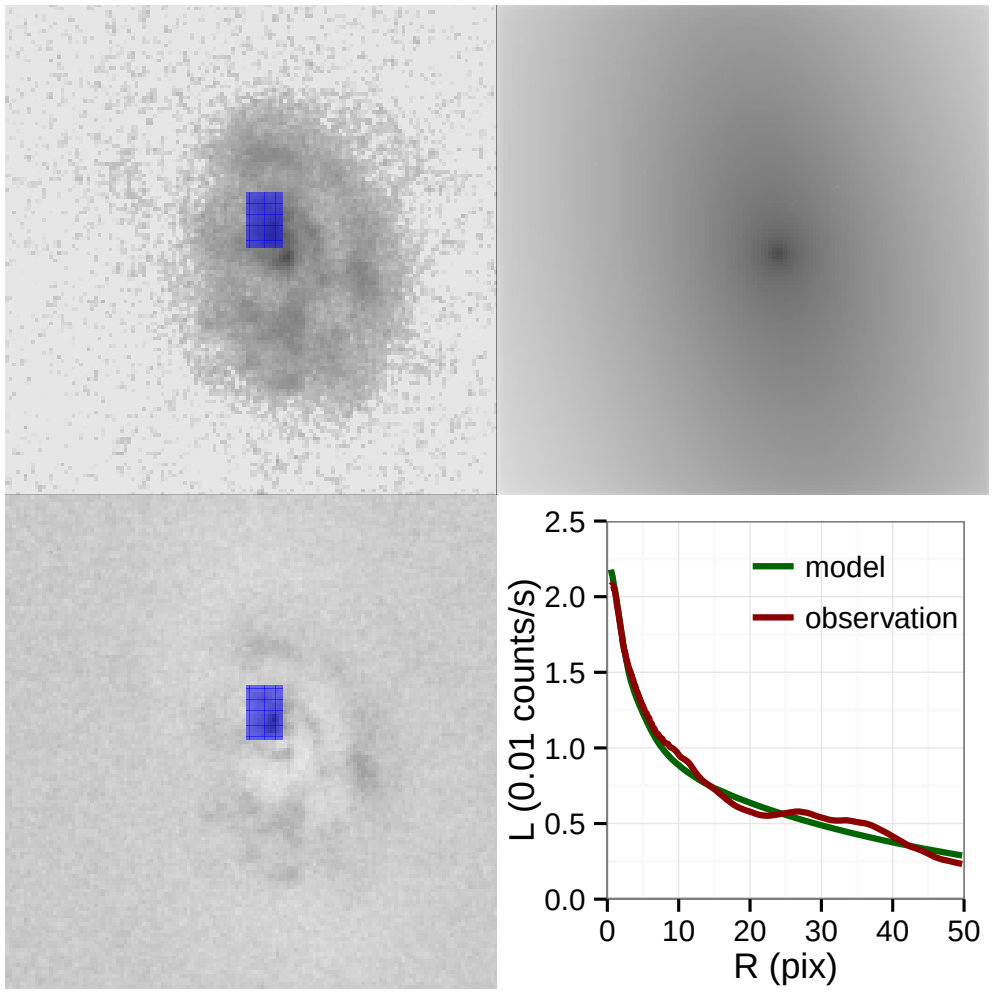

Figure 5.1: An illustration of a typical photometric fitting. The top left panel is observed galaxy, where blue colour denotes masked out region. Top right panel shows model image, bottom left their difference. Bottom right panel shows the luminosity profile along the major axis of the observed (red) and modelled (green) image.

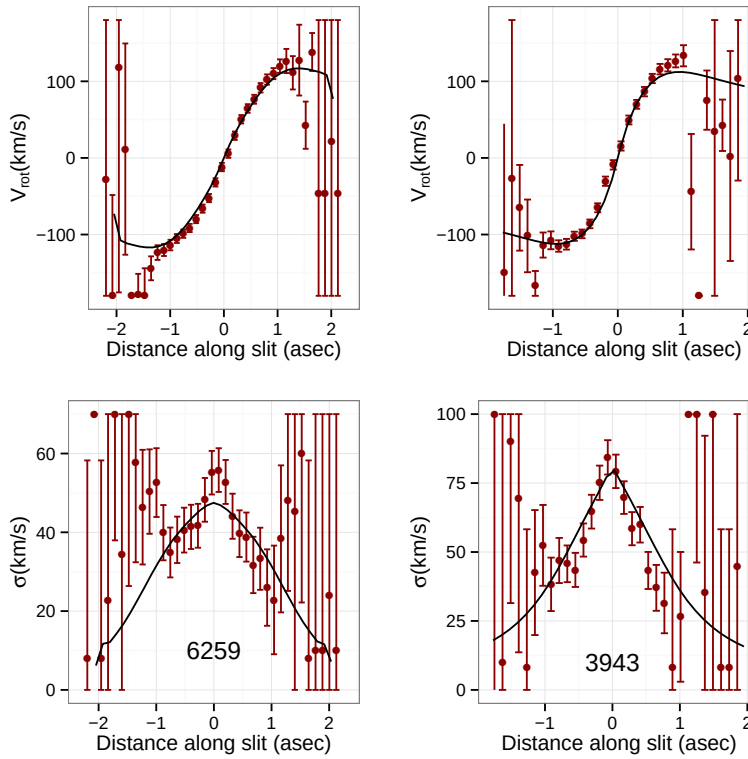

Figure 5.2: Typical fits for two galaxies: left one is for galaxy TKRS 6259 (the nomenclature is the same as in Weiner et al. (2006)), and the right for TKRS 3943. Top panels show rotation curve while the bottom ones velocity dispersion distribution. Due to high computational time, the fitting was done by hand.

could use mainly the dispersions to find the gas disc parameters, reducing available data and therefore the model accuracy even more. Despite the issues, the modelling could be done with some accuracy. An example of the results of kinematic fitting can be seen in Figure 5.2.

A direct estimation of the uncertainties of each free parameter and of the calculated gas disc thicknesses $h_{\rm g} = q_{\rm g} a_{0,{\rm g}}$ was complicated because of the very long calculation time required for each iteration. For each galaxy, the quality of the model was estimated according to the residuals of both the kinematic and photometric fits, based on what some galaxies were considered to have too poor fit to have reliable model parameters.

One important source of the error of the gaseous disc parameters is the uncer-

tainty of the inclination angle. The inclination angle and the thickness of a component are degenerated, hence the thickness of the stellar disc is affected considerably by photometric modelling errors. To a certain extent, this degeneracy influences also the determination of gas disc thickness. We estimated the influence of this degeneracy on the galaxy TKRS 760, a galaxy that represents a typical galaxy in our sample. It has an average apparent isophote axial ratio $Q = 0.53$. While varying the intrinsic axial ratio of the stellar disc from $q = 0.1$ to 0.3 the corresponding inclination angle became $\gamma = 59^\circ - 64^\circ$ and the calculated gas thickness $h_\mathrm{g} = 0.99 - 1.43$ kpc. This uncertainty estimate does not include the error from spectrograph CCD pixel binning (the locations of the bins, to be exact), which by our calculations is important to consider during the gas kinematic modelling.

Although the errors of the single galaxy parameters are enormous, the average over the sample can give some insights into the galaxy evolution. Tables 5.1 and 5.2 give the results of parameters acquired by the dynamical fitting of gas. Recent works based on kinematics of different gas indicators suggest that there exist thinner and thicker gas populations (Mogotsi et al. 2016). Our results describe the higher dispersion – thicker one.

The conclusion of the application of dynamical modelling is that in principle it can be applied, but there is the requirement for kinematical observations to have high resolution and signal-to-noise ratio.

5.2 Modelling of an example galaxy – Andromeda galaxy

In this section we compare the results of our stellar dynamic model described in Chapter 2, with observations to see how good this model is in practice. For this purpose, we chose a well studied galaxy, M31, that has excellent kinematic observations and the density distribution is firmly known from photometric observations.

5.2.1 The data and assumptions for the dynamic model

Similarly with the dynamical model of gas, the first step was to find the density distribution for the Andromeda galaxy. It has been done many times, for example by Geehan et al. (2006); Seigar et al. (2008); Chemin et al. (2009); Corbelli et al. (2010), but for our purposes Tamm et al. (2012) seems most appropriate: it found the mass distribution mostly from dust-corrected photometry, making mass estimation independent of stellar kinematics. The dark matter in Tamm et al. (2012) was found by fitting the rotation curve of gas with observed components with the added dark matter halo. Since the gas rotation is semi-independent of stellar kinematics (gas kinematics usually give only the upper limit for the stellar rotation curve), we have comparison

Table 5.1: Derived best-fit parameters of the modelled galaxies for stellar components. "…" indicates that modelling did not converge to a solution.

			Bulge				Stellar disc			
id	z	γ	a_0	q	N	M	a_0	q	N	M
		deg	kpc			$10^{10}\mathrm{M}_\odot$	kpc			$10^{10}\mathrm{M}_\odot$
760	0.503	62	0.93	0.90	2.9	0.20	3.5	0.203	0.64	0.31
2514	0.682	60	1.89	0.80	4.4	…	3.8	0.203	2.36	…
3943	0.484	62	1.06	0.93	4.0	0.20	3.3	0.207	0.79	0.75
4023	0.280	88	3.03	0.76	6.0	…	6.6	0.169	1.08	…
4210	0.503	65	0.97	1.00	4.0	0.30	5.4	0.203	0.75	0.36
4387	0.503	62	0.98	0.95	4.3	0.80	7.3	0.212	0.85	1.00
4467	0.355	60	1.00	1.00	4.0	2.00	6.1	0.200	1.00	1.96
4822	0.398	30	0.58	0.75	3.7	0.30	4.7	0.200	1.63	0.94
5619	0.681	59	1.28	0.95	4.8	0.17	6.6	0.198	0.74	0.20
5707	0.840	60	1.85	0.87	6.7	0.20	8.0	0.197	0.62	0.53
5785	0.841	13	1.10	0.93	4.0	…	1.0	0.300	4.04	…
5789	0.139	55	0.62	0.99	1.6	…	3.4	0.222	0.68	…
6259	0.337	70	1.02	0.95	4.0	0.20	4.0	0.152	0.32	0.63
6281	0.835	49	0.99	0.84	5.8	7.00	5.5	0.203	1.95	1.32
6627	0.484	75	0.95	0.95	7.0	…	4.6	0.194	1.75	…
6858	0.079	40	0.76	1.00	2.6	0.05	3.8	0.200	0.81	0.10
7187	0.840	68	0.42	1.00	2.6	0.50	8.6	0.253	0.68	0.76
8015	1.016	64	4.19	1.00	6.7	1.00	14.3	0.200	1.00	8.00
9012	0.254	90	1.75	0.94	3.7	0.10	7.5	0.113	0.93	0.89
9059	0.253	56	1.13	0.32	4.0	…	5.0	0.171	0.47	…
9316	0.438	56	1.08	0.69	3.4	1.20	2.5	0.229	0.99	0.20
9575	0.561	52	3.28	0.91	5.0	1.00	6.2	0.205	1.29	1.43
9635	0.114	53	1.13	1.00	5.4	…	1.8	0.157	0.51	…
9932	0.087	62	0.90	0.90	2.9	0.02	2.1	0.203	0.76	0.05
10513	1.140	73	0.89	1.00	3.9	0.05	6.7	0.199	1.34	0.26
10683	0.475	76	0.73	0.96	6.0	1.00	5.1	0.272	0.64	3.89
10811	0.422	77	1.00	1.00	4.0	0.00	5.4	0.200	1.91	0.95

Table 5.2: Derived best-fit parameters of the modelled galaxies for "invisible" components. "..." indicates that modelling did not converge to a solution. The dark matter density ρ_0 is measured in units of $10^{10}\mathrm{M}_\odot\mathrm{kpc}^{-1}$.

			Gas disc				DM
id	z	γ	a_0	h_g	N	M	$\log\rho_0$
		$^\circ$	kpc	kpc		$10^{10}\mathrm{M}_\odot$	
760	0.503	62	4.9	1.24	0.64	0.25	-6.1
2514	0.682	60	5.4	...	2.36	1.73	...
3943	0.484	62	4.6	0.88	0.79	1.08	-6.3
4023	0.280	88	4.9	...	0.64	0.25	...
4210	0.503	65	7.6	0.98	0.75	0.29	-6.1
4387	0.503	62	10.3	0.62	0.85	0.60	-5.5
4467	0.355	60	8.5	0.26	1.00	0.29	-5.6
4822	0.398	30	6.6	1.33	1.63	0.83	-5.5
5619	0.681	59	9.3	2.50	0.74	0.02	-6.8
5707	0.840	60	11.2	0.78	0.62	0.27	-6.9
5785	0.841	13	4.9	...	0.64	0.25	...
5789	0.139	55	4.9	...	0.64	0.25	...
6259	0.337	70	5.5	0.61	0.32	0.12	-6.8
6281	0.835	49	7.7	3.87	1.95	0.37	-6.8
6627	0.484	75	4.9	...	0.64	0.25	...
6858	0.079	40	5.3	0.69	0.81	0.12	-6.5
7187	0.840	68	12.0	1.44	0.68	0.08	-5.9
8015	1.016	64	20.1	2.41	1.00	2.00	-5.6
9012	0.254	90	10.1	0.90	0.93	0.01	-5.8
9059	0.253	56	7.0	...	0.47	0.02	...
9316	0.438	56	3.5	0.42	0.99	0.01	-6.2
9575	0.561	52	8.7	2.19	1.29	0.07	-6.1
9635	0.114	53	2.6	...	0.51	0.12	...
9932	0.087	62	3.0	0.06	0.76	0.07	-7.8
10513	1.140	73	9.4	1.31	1.34	0.04	-6.1
10683	0.475	76	7.1	1.64	0.64	0.18	...
10811	0.422	77	7.6	1.67	1.91	0.77	-5.7

Table 5.3: Mass distribution model parameters of M31, taken from Tamm et al. (2012). The parameters for each component correspond to the density distribution Eq. (4.2).

Component	a_c kpc	q	N	ρ_c $M_\odot \mathrm{pc}^{-3}$	M $10^{10} M_\odot$
Bulge	2.025	0.73	4.0	0.220	4.9
Disc	11.35	0.10	1.0	0.017	4.8
Dark matter	178	1.00	6.0	8.12×10^{-6}	205.6

Table 5.4: Best-fit values of the free parameters of the model. Parameters a_2, b_2 and z_0 describe the shape and orientation of the velocity ellipsoid, β sets rotation velocities of the stellar components. The indicated errors are standard deviations derived directly from the bayesian analysis tool *multinest*.

Parameter	Bulge	Disc
a_2	0.11 ± 0.004	0.41 ± 0.002
b_2	0.01 ± 0.04	0.04 ± 0.02
z_0	9.8 ± 4.0	11.5 ± 0.3
β	0.32	0.95

data that did not affect the estimation of the density distribution. The density distribution is described with superposition of Einasto profiles, the corresponding parameters are in Table 5.3.

The second step for applying the model is to get the Jeans equations consistent with the third integral of motion. It is implemented by minimising Eq. (2.42). We chose to use a Bayesian approach, where from the shape of the posterior distribution we found the values and statistical errors for the resulting parameters. This statistical method is implemented in the Multinest code (Feroz & Hobson 2008; Feroz et al. 2009, 2013).

As there are two kinematically very different components in the Andromeda galaxy (the bulge is dominated by random motions, while the disc is rotation supported) we have to fit the consistency for each component separately. An image describing the resulting consistency can be found in Figure 5.3 and the corresponding parameters of the model in Table 5.4. In the table, the statistical errors that are acquired by finding the standard deviation from the posterior distribution are also presented.

One intermediate result of the dynamical model is the shape and orientation of the velocity dispersion tensor. The shape of it is presented in Figure 5.4. A major

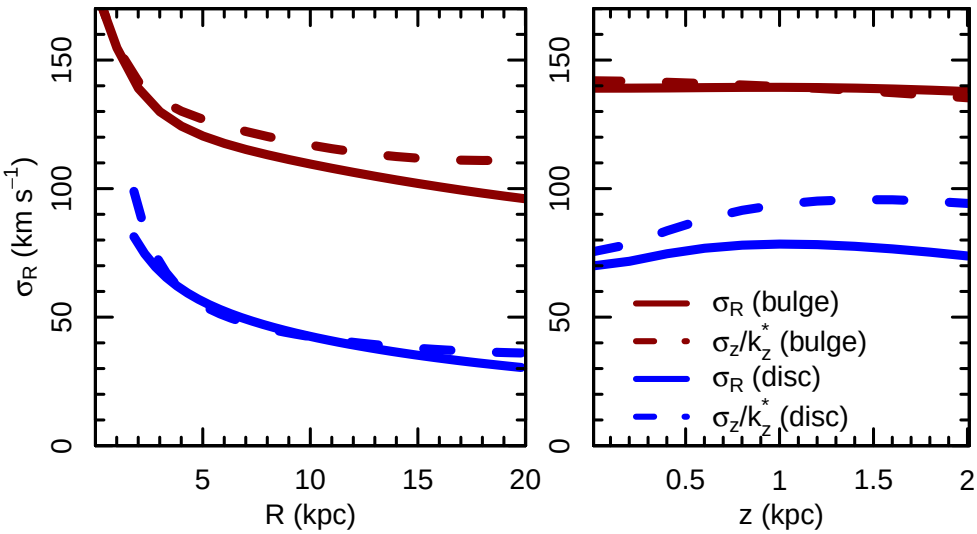

Figure 5.3: The consistency of Jeans equations (2.36) and (2.37) with the assumption of correctness of the third integral theory. The consistency is found for each component separately: for the bulge, the consistency is excellent, and for disc it is good.

problem of the dynamical modelling is the unknown constraints to the velocity ellipsoid: we have enough data only to find the kinematics in our Galaxy, which is the reason we compare the model dispersion ratios of M31 with Milky Way ones. Further discussion about the dispersion tensor can be found in Section 2.3.1.

5.2.2 Comparison of the model stellar kinematics with observations

We have the means to find the model kinematics that mimic the observations once the density distribution is fixed and Jeans equations have been made consistent with the third integral of motion. For direct comparison over the line of sight integration was done as described in Section 3.1.2, but due to proximity of the neighbouring galaxy no additional effects, such as seeing or the smearing of the slit of spectrograph was taken into account.

We chose to compare model kinematics with the observed ones in three different regions: on the major axis, above and below the major axis in disc, and in the galaxy bulge region.

The comparison observations on the major axis were taken from McElroy (1983), Kormendy (1988), van der Marel et al. (1994), and Kormendy & Bender (1999). To improve the readability of the plot, we combined the observations as was done in

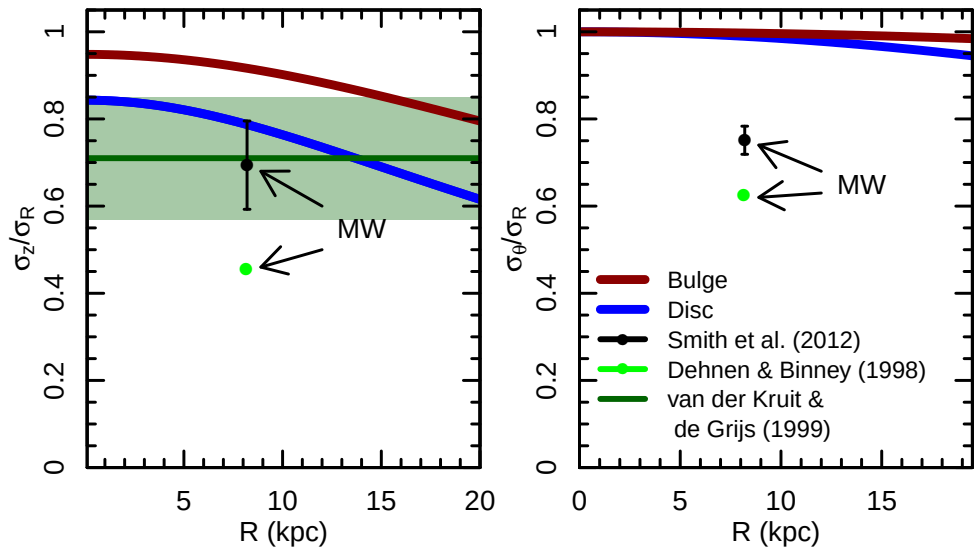

Figure 5.4: The shape of the velocity dispersion ellipsoid described by the vertical to radial and azimuthal to radial ratios of velocity disperions. The comparison points are from our Galaxy observations (Dehnen 1998; Smith et al. 2012) and should be compared with the disc line, or from other galaxies using known correlation between various parameters (van der Kruit & de Grijs 1999).

Tempel et al. (2007). It is possible to acquire additional kinematic comparison data if we assume the similarity of the kinematics of planetary nebulae and stars. Since the planetary nebulae are just a short epoch of the evolution of star, they have the same kinematics. The data from Halliday et al. (2006) and Merrett et al. (2006) contain the planetary nebulae kinematics. We show the resulting model and observational kinematics in Figure 5.5. The kinematics can be calculated in two ways: finding σ_R or σ_z from Eq. (2.36) or (2.37) respectively, and use the third integral theory to determine all other components of dispersions. The model kinematics found with these two methods are represented in the figure with black and grey lines. As the consistency fitting was not perfect, these lines do not match exactly. Since the difference of the lines is smaller than errors from observations, we consider them both in accordance with observations. The inconsistency of the model and observed kinematics in the central and outer regions are caused by the lack of stellar halo and nucleus of the model.

Figure 5.3 shows that the bulge region is better described by the model than disc. To test whether this shows also in consistence in observations and model, we compared our model with the Saglia et al. (2010) observations. They observed the bulge with six different position angles going through the centre of the galaxy. The model comparison with observations can be seen in Figure 5.6. It is seen that on major axis, the consistency is excellent, while on other regions only good meaning the consistency fitting with different components is justified and the model is well applicable.

Finally, to see how well our model works outside the galactic plane, we compared the model and observations above and below the major axis of the M31, where the light from galactic plane dominates slightly less. The comparison observations come from Zou et al. (2011) paper, and the results are seen in Figure 5.7. The high similarity of the model and observations is seen, again confirming the suitability of the dynamic model even outside the galactic plane.

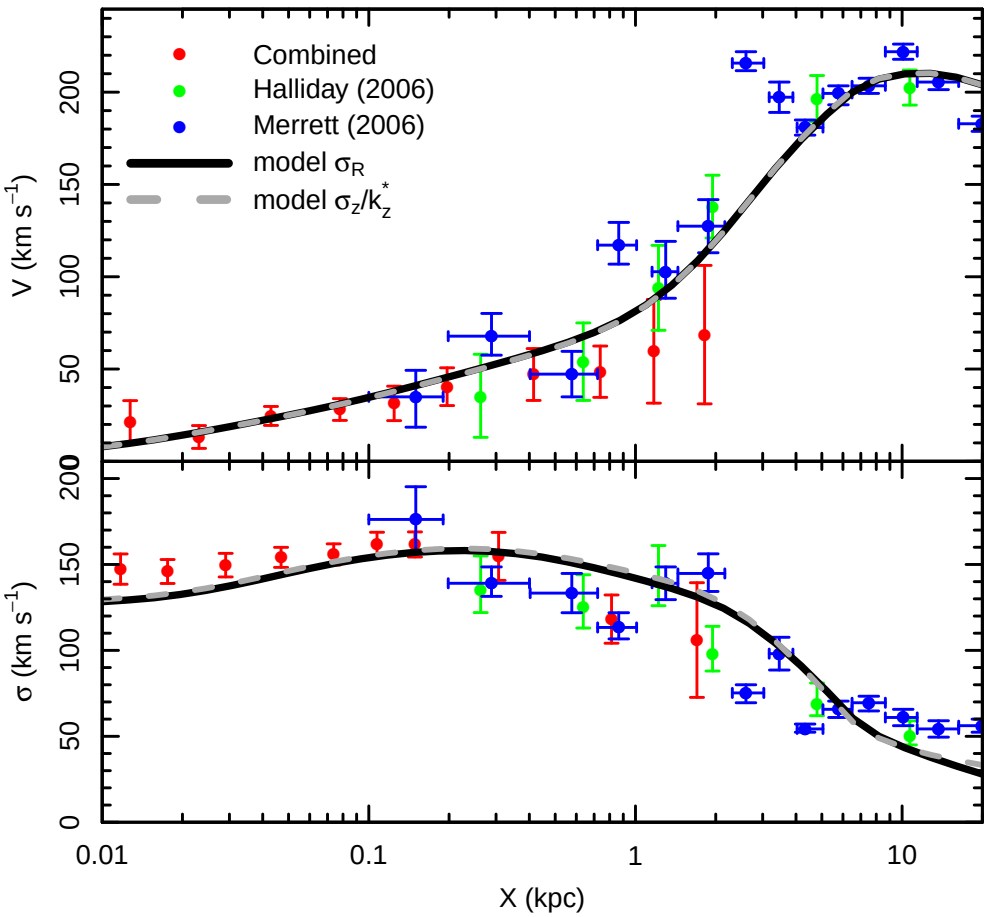

Figure 5.5: The observed and model kinematic comparison on the major axis. The observations of the combined data points come from McElroy (1983), Kormendy (1988), van der Marel et al. (1994), and Kormendy & Bender (1999) from stellar observations. Halliday et al. (2006) and Merrett et al. (2006) show the kinematics of planetary nebulae, which mimic the motion of stars.

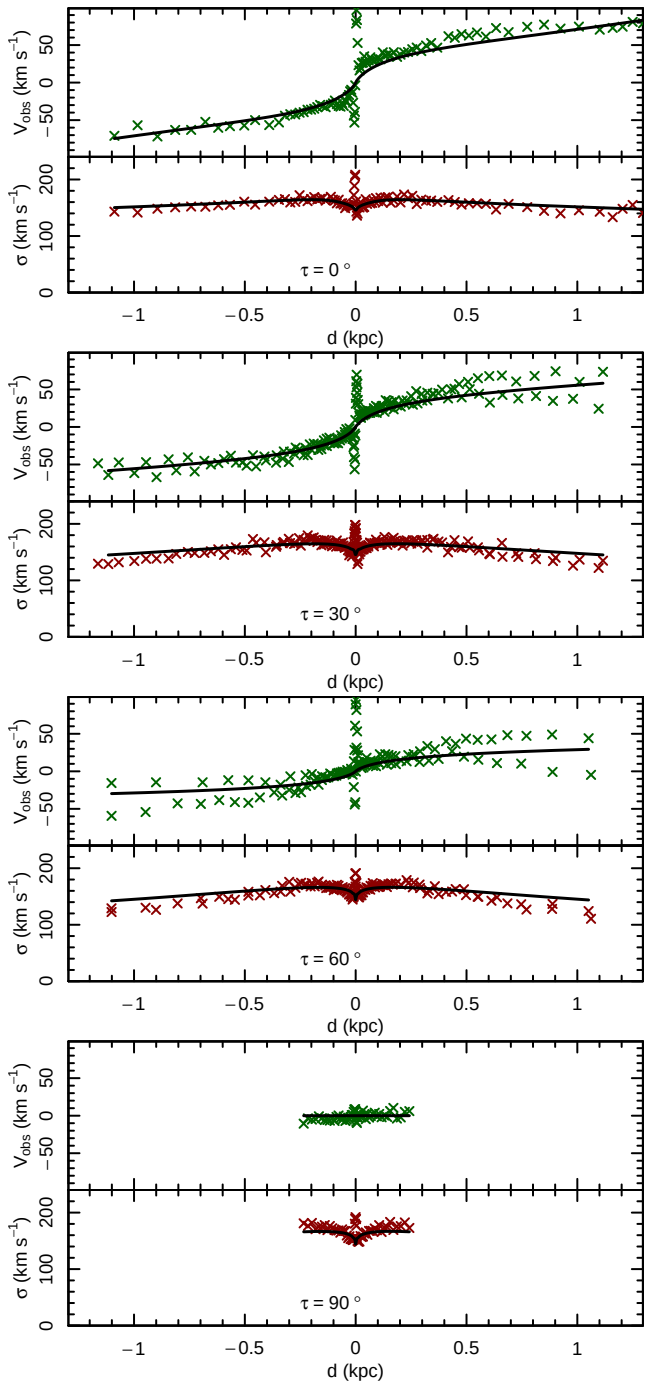

Figure 5.6: The comparison of the kinematic model and observations near the bulge with different spectrograph slit position angles (for illustration, see figure 1 from Saglia et al. (2010)). The τ in each panel shows the angle between the major axis of galaxy and the spectrograph slit position. $\tau = 30°$ and $\tau = 60°$ show two sets of observed lines that originate from different sides of the major axis. The central peaks in velocity and dispersions are disturbed kinematics of the supermassive black hole, which usually affects kinematics within a few tens of parsecs from it.

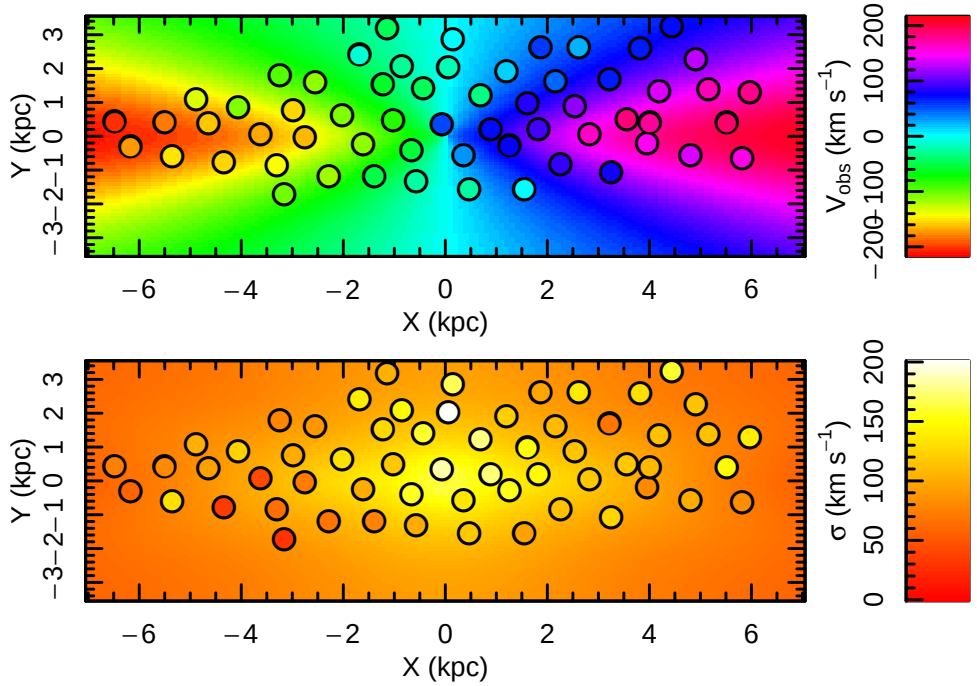

Figure 5.7: The comparison of the observed and model kinematics based on Zou et al. (2011) data: the top panel shows rotational velocity while the bottom one the velocity dispersions. The background of the images shows the model values, while the inside of circles observational results.

CHAPTER 6
DUST EFFECTS IN THE OBSERVED KINEMATICS OF A GALAXY

In previous sections we developed a model to describe the kinematics of a galaxy at each point (Sect.3.1). We described how the line of sight integration changes observed rotation velocities and dispersions (Sect.3.1.1). To study how the attenuation due to dust affects the observed kinematics, we use the previous results and apply the model to the Andromeda galaxy.

The influence of the dust absorption on the galaxy kinematics is not a well studied field. It is quite often handled as a secondary effect in case of low inclination galaxies. In addition, there are only a few good kinematical models being capable of describing galaxy kinematics outside of galactic plane. A great effort has been made by Baes & Dejonghe (2000), who used a two-integral model to describe elliptical galaxies and derived that it is important to take into account dust absorption when face on optical depth $\tau > 5$. They also found that very thick and very thin dust discs do not significantly influence galaxy kinematics. For disc galaxies Baes et al. (2003) derived that dust may have a severe effect in edge-on galaxies, but the effect reduces remarkably when the inclination angle of a galaxy changes even by a few degrees. Thus, the dust may influence the kinematics of galaxies and it is important to take it into account.

6.1 The effect of the dust attenuation to model kinematics

In order to calculate how dust absorption influences the kinematics of a galaxy, one has to assume how the dust is distributed within a galaxy. We describe dust distribution with the dust attenuation coefficient κ_{d}, a coefficient used to calculate the optical depth $\tau = \int_{\mathrm{los}} \kappa_{\mathrm{d}}$ on the line of sight and therefore light dimming distribution in a galaxy. Now we need to select a profile describing the dust attenuation coefficient distribution. There are many motivated profiles, such as a double exponential model, a sandwich model, an exponential model with a central hole etc to describe dust distribution in a galaxy. We decided to use a double exponential distribution model as is it sufficiently flexible and has at the same time quite a small number of free parameters. In addition, it is widely used to describe the dust (e.g. Xilouris et al. (1999); Bianchi (2007); Viaene et al. (2015)), allowing to constrain possible range of profile parameters from studies of other galaxies. The formula for double exponential profile

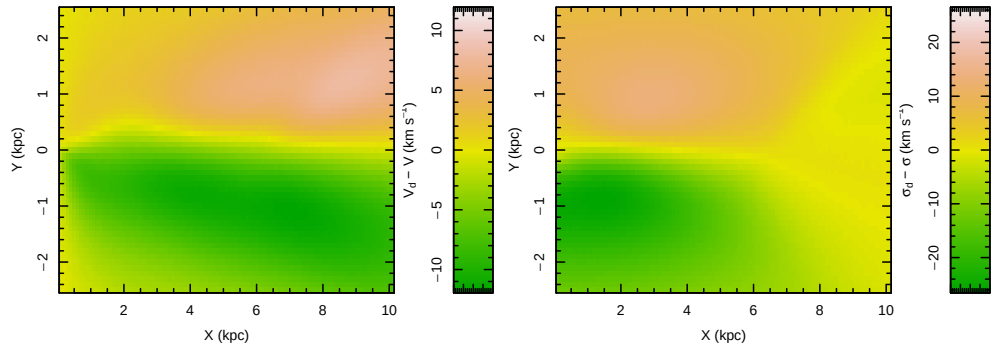

Figure 6.1: The kinematical differences of the dusty and dustless galaxy. The left panel shows the difference of observed velocity in percentages $(V - V_{\rm dust})/V$ while the right panel dispersion difference $(\sigma - \sigma_{\rm dust})/\sigma$. For the test model parameters, the differences in both velocity and dispersion are less than 25%, being higher in the central and dusty region and almost irrelevant on the outer regions of the galaxy.

for the attenuation coefficient is:

$$\kappa_{\rm d} = \frac{\tau_0}{2z_{\rm d}} \exp\left(-\frac{|z|}{z_{\rm d}} - \frac{R}{R_{\rm d}}\right), \tag{6.1}$$

where $z_{\rm d}$ and $R_{\rm d}$ are the scale height and scale length of the dust distribution, τ_0 is the optical depth at the centre of a face-on galaxy. Xilouris et al. (1999) and Bianchi (2007) derived that dust disc is usually from $1/3$ to $1/2$ times thinner than the stellar disc and radially approximately $\sim$ 1.5 times more extended than the stellar disc. The value for the optical depth cannot be determined uniquely since it varies with the wavelength (described by the Calzetti curve). Although no unique value can be determined for the whole optical range, Bianchi (2007) estimated τ_0 to be $0.5 \ldots 1.5$ in V band.

As our purpose was not to model the dust distribution and properties in M31, but to give quantitative estimates to the dust absorption effects, we only need an approximate dust distribution profile. On the basis of the papers referred above (Xilouris et al. 1999; Bianchi 2007) we fixed the dust disc with the following parameter values: $z_{\rm d} = 0.3{\rm kpc}$, $R_0 = 11.9{\rm kpc}$, and the $\tau_0 = 3$.

The calculated effect of the dust absorption on the rotation and dispersion curves of a galaxy can be seen in Figure 6.1. It is seen that the distribution of the $\Delta V/V = (V - V_{\rm dust})/V$ is not symmetric with respect to ΔV suggesting that if we ignore dust effects on velocities, also galaxy masses ($\Delta M/M \sim 2\Delta V/V$) may be systematically underestimated. Thus, the real masses of galaxies can be larger than model estimates. One can notice from Figure 6.1 that on the major axis, the rotation and dispersions

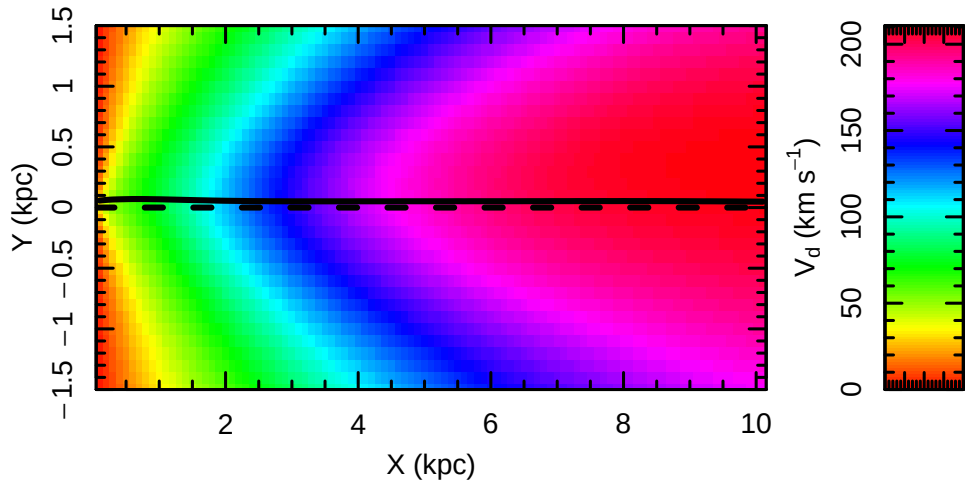

Figure 6.2: This illustration shows the change of the kinematic major axis in case of dusty galaxy. The dashed line shows the real major axis passing through the galaxy centre along the position angle. The solid line shows the region, where rotation is the highest – kinematic major axis. One can see these lines do not match.

are less affected by the dust. This is caused by the symmetry of kinematics in front of and behind the dust layer. To have accurate results slit of the spectrograph must be oriented with maximum precision.

A qualitative indication of the dust affecting the observed kinematics can be seen in Figure 5.6 in the two middle panels: a distinctive vertical difference can be in the data points with the same X. The data points originate from each side of the major axis (same X value, but $\pm Y$), showing similarity with kinematics in Figure 6.1 and therefore suggesting the presence of dust.

The asymmetry of the kinematical parameters above and below the major axis causes maximal rotation/dispersion values to vary with major axis (when there is no dust absorption the maximum is located on the major axis). We derived that the location of the major axis (or equivalently position angle ϵ) calculated from kinematics may be affected by dust absorption and may vary with the distance from the galaxy centre. This is seen in Figure 6.2. On the other hand, variation of the position angle of the kinematic major axis can be explained also when the bulge is assumed to have a three-axiality symmetry (Saglia et al. 2010).

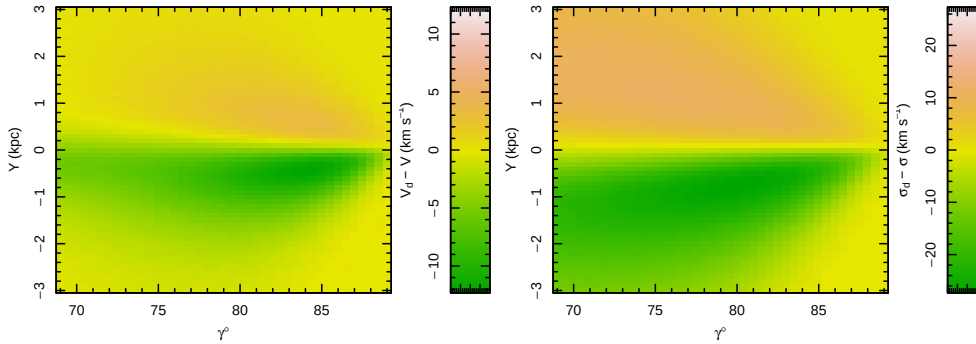

Figure 6.3: The difference of measured velocities and dispersions with and without dust depending on inclination angle γ. The kinematics are measured in slices parallel with minor axis and with fixed $X = 1.2$ kpc. The other model parameters were fixed to $\tau_0 = 3$, $R_\mathrm{d} = 11.9$ kpc and $z_\mathrm{d} = 0.3$ kpc. In the figure, it can be seen that the dust effect rises sharply when galaxy is more inclined than $\sim 80^\circ$ up to 25% difference, while there is small dependence on the intermediate and small inclinations.

6.2 Dependence of rotational velocities and velocity dispersions on the dust disc parameters

As the kinematics of galaxies are used in many applications, e.g. Tully-Fisher relation and mass calculations, it is important that we are able to quantify the dust effect. For a test object we selected a typical disc galaxy in a nearby universe, an M31 like galaxy and varied dust disc parameters and the inclination angle of the galaxy.

The most volatile parameter describing the galaxy is the inclination angle. One can see from Figure 6.3 that galaxy kinematics variations due to dust are quite sensitive to the inclination of a galaxy. It is seen that for higher inclinations dust attenuation becomes more and more important and regions with the strongest effects move closer to the galactic plane. The latter can be explained by the increase of flatness of the galaxy in the plane of the sky. The influence of the dust is significant in galaxies with inclination angles $\gamma > 80^\circ$. Unfortunately, the fraction of galaxies with these inclination angles is over 15%, making the effect statistically quite important.

Next we studied dust effects due to variation of the optical depth τ_0 i.e. the amount of dust. Figure 6.4 demonstrates how much the amount of dust changes the kinematics. It is evident that kinematics change drastically when the optical depth changes. A reason for it could be the changes in the observed wavelength, a relation sometimes called the Calzetti curve, and it indicates that in optical wavelength range, the κ_d can vary ~ 2 times (Calzetti 1999; Xilouris et al. 1999). Thus, together with previous results it is clear that one cannot measure a single velocity profile along a

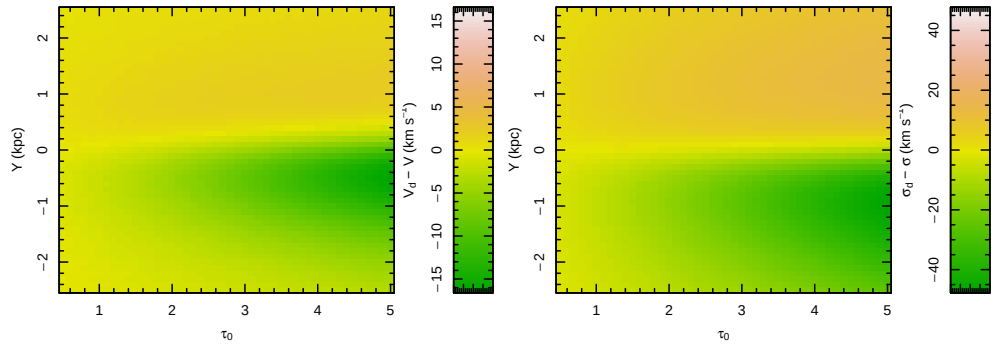

Figure 6.4: Kinematic difference of the line of sight velocities and dispersions with and without dust as a function of optical thickness τ_0. The kinematics are measured in slices parallel with minor axis and with fixed $X = 1.2$ kpc. From the optical depth $\tau_0 > 1$ shows remarkable increase in the error of the kinematics. The non-varying model parameters were fixed to $z_\mathrm{d} = 0.3$ kpc and $R_\mathrm{d} = 11.9$ kpc.

line of sight in case of dusty galaxy, making kinematic modelling extremely difficult. From Figure 6.4, one can also see that one side of galaxy is more affected than the other one. This does not depend on optical depth. We interpret this in a way that even in case of substantial dust amounts we can always see the light that originates above the dust lane. This effect becomes smaller when the dust disc thickness parameter z_0 increases.

The last parameter we study is the thickness of the dust disc. Figure 6.5 shows how kinematical characteristics of a galaxy depend on the thickness of the dust disc. One can see that in case of thinner dust discs, the kinematical characteristics are more influenced by dust. In case of thick dust disc the higher and lower parts of the luminosity distribution have similar (but not the same) proportions, while in case of the thin dust disc the parts high above the plane and nearer to us dominate in the luminosity and in the kinematics. As we mentioned already, from Xilouris et al. (1999); Bianchi (2007) we may take dust and stellar disc thickness ratio $\sim 1/3 \ldots 1/2$ suggesting that dust disc thickness $z_\mathrm{d} \simeq 0.3$ is realistic for M31 model.

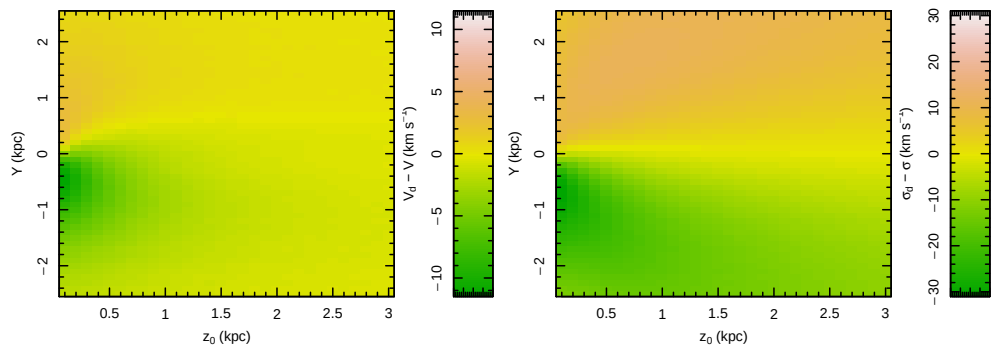

Figure 6.5: Kinematic difference of the line of sight velocities and dispersions with and without dust as a function of dust disc thickness $z_{\rm d}$. The kinematics are measured in slices parallel with minor axis and with fixed $X = 1.2$ kpc. It is seen that the thinner the dust disc, the higher the kinematic distortion, thicker discs show an existing, but smaller dependence. The non-varying model parameters were fixed to $\tau_0 = 3$ and $R_{\rm d} = 11.9$ kpc.

CHAPTER 7
SUMMARY

The aim of the present Thesis was to develop a method to study the dynamics of galaxies and various effects that could affect the comparison of the model calculations with observations and to test the developed model.

The dynamic model is the means to find kinematical descriptive functions of a galaxy (rotation velocities and velocity dispersions) by knowing the density or gravitational potential distribution of the galaxy. Usually a galaxy is assumed to consist of several different components. The behaviour of various components can be different even within the same conditions – e.g. gas has isotropic velocity dispersion distribution, while stellar components do not. Therefore, different models should be used for different components. In the present Thesis, Jeans equations are used for dynamical modelling.

The modelling of gas kinematics by using Jeans equations is rather straightforward as the equations have a unique solution. In case of modelling the dynamics of a stellar component, models need to be much more sophisticated. The nearly collisionless nature of the stellar motions does not allow to solve the Jeans equations separately and equations must be handled as a system. In addition, a number of unknown functions in these equations is greater than the number of available equations. The most important result of this Thesis is demonstrating that when using the third integral of motion to constrain the velocity dispersion ellipsoid it is possible to solve the Jeans equations separately. We used the form of the third integral derived by Kuzmin (1953, 1956) and took other integrals of motion into account according to Einasto (1970).

By solving the Jeans equations for a given density distribution we can calculate rotation velocities and velocity dispersions at all points within a galaxy. To compare our model calculations with observations, we have to mimic the reality further. There are various modifications needed for it, the first one is to take into account all the points on each line of sight. Next, two additional effects, the smearing of image (convolution) due atmospheric turbulences and due to the slit width of a spectrograph are needed to take into account. This is especially important if the apparent sizes of galaxies in the sky are comparable to the slit width and/or seeing point spread function.

The prerequisite of any dynamic modelling is the knowledge about the baryonic and the dark matter distribution inside a galaxy. We studied how well the parameters of stellar light distribution can be recovered by creating a set of test-galaxies and remodelling them. The reassuring result is that the luminosity (proportional to the

stellar mass) distribution can be recovered rather well and also the inclination angle that is vital to model the dynamics of a galaxy is adequately restored. The bulge-to-disc ratio is well recovered in case all the components are being represented well. Fortunately, if one component dominates, the smaller component is usually irrelevant for the kinematic modelling. A problem arises when we try to recover the flatness and inclination angle of a component. This can be done with the absolute accuracy of ~ 0.1, hinting possible rather high uncertainties in case of the dynamic modelling of some galaxies.

For testing our gas dynamic models, we selected a sample of galaxies at moderate redshifts. Our aim was to study the thicknesses of gaseous discs. We concluded that in principle, the kinematic modelling can be done for these galaxies, but one has to be very careful due to additional observational effects. Images of these distant galaxies are small being comparable to the slit width of the used spectrograph and also comparable to atmospheric seeing, making the result slightly uncertain. To test the stellar dynamic model calculations, the model was applied to the Andromeda galaxy, M31. We found that concordance of the model calculations with the observations was remarkable, considering the model is calculated without taking into account the observed stellar kinematics.

One further application of the developed model was to study how much the attenuation due to dust affects the observed kinematic quantities – the rotational velocity and velocity dispersions. Assuming a typical dust disc within a galaxy we derived that rotational velocities were changed by $\lesssim 10$ km s^{-1} and dispersions by $\lesssim 20$ km s^{-1}. The presence of a dust disc has the most significant effect in the central regions of a galaxy and above or below the major axis of a galaxy on the kinematics, hence also to the mass. Our results show that the change in velocity dispersions is much more wide-spread than the change in rotational velocity.

The model developed in the present Thesis can be used to model the kinematics by using data all over the apparent image of a galaxy – the information we are starting to obtain within the era of integral field spectroscopy. We would like to mention CALIFA (Sánchez et al. 2012), MANGA (Bundy et al. 2015), TKRS2 (Wirth et al. 2015) etc surveys being ongoing or prepared. We can apply our model on all galaxies in these surveys.

CHAPTER 8
KOKKUVÕTE (SUMMARY IN ESTONIAN)

Galaktikate modelleerimine: dünaamilised meetodid ja rakendused

Käesoleva doktoritöö eesmärk oli välja töötada meetod, millega on võimalik modelleerida galaktikate dünaamikat. Samuti sai seatud eesmärgiks arvesse võtta ja hinnata võimalikke efekte, mis mõjutavad mudel- ja vaatlusandmete omavahelist võrdlemist.

Dünaamilise mudeli eesmärk on leida osakeste liikumine, kui on ette antud galaktika mitmekomponendiline tihedusjaotus (või ekvivalentselt gravitatsioonipotentsiaali jaotus). Kuna gaas ja tähed käituvad samades tingimustes erinevalt (gaasi põrkelise olemuse tõttu), siis on tarvis eristada neid juhte vastavalt rakendatavale komponendile. Seetõttu oli vaja arendada oma modelleerimise meetod mõlema komponendi jaoks. Antud töös kasutasime mõlema komponendi dünaamika kirjeldamiseks Jeansi võrrandeid.

Esmalt uurisime gaasi käitumist galaktikate potentsiaalis. Kuna gaasi osakesed põrkavad teiste gaasi osakestega, siis iga põrke käigus kiiruse suunad juhuslikustatakse, mistõttu on gaasi osakeste kiiruste jaotus isotroopne. Vastav seos võimaldab märkimisväärselt lihtsustada Jeansi võrrandeid ning need ka lahendada. Teine dünaamiline mudel, mida on antud doktoritöös käsitletud, kirjeldab tähtede liikumisi. Stellaarse dünaamika mudeli koostamise keerukus seisnes Jeansi võrrandite sulgemises: olemasolevaid võrrandeid on vähem kui muutujaid, mistõttu lahend pole ühene. Lisaprobleem on tihedusjaotuse kõdumine kiiruste jaotuse anisotroopsusega. Doktoritöö üks põhitulemus on, et me lahendasime Jeansi võrrandid, kasutades Kuzmini kolmanda integraali teooriast tuletatud seoseid kiiruste ellipsoidi kujule. Meetodi puudus seisneb arvutusmahukate Jeansi võrrandite kooskõlla viimises kolmanda integraali teooriaga, mida alati ei saa teha täpselt.

Jeansi võrrandite lahend annab meile kinemaatilised suurused igas galaktika punktis, kuid sellest tulemusest ei piisa saamaks pädevat võrdlust vaadeldud kinemaatika ja mudeli vahel. Korrektseks võrdluseks on vaja arvestada, et tavaliselt on galaktikad läbipaistvad ning kõik punktid, mis jäävad vaatejoonele, tuleb arvesse võtta. Kaks olulist lisaefekti on atmosfääri turbulentside ja spektrograafi pilu tõttu tekkiv mudelpildi konvolutsioon. Eriti oluline on see arvesse võtta galaktikate korral, mis paistavad taevas väikestena.

Enamiku dünaamilise modelleerimise rakenduste alguspunktiks on massijaotuse leidmine, mida antud töös kirjeldame kolme või nelja komponendi summana: täheline mõhn, täheline ketas, tumeaine halo ning vastavalt mudelile ka gaasiketas. Täheliste komponentide parameetrid, mida me kirjeldasime Einasto tihedusjaotusega, on leitavad fotomeetriliste andmete põhjal. Doktoritöö 4. peatükk vaatleb, kui täpselt on

võimalik taastada galaktika tähelise jaotuse parameetreid fotomeetrilise modelleerimise põhjal. Selleks konstrueerisime mudelgalaktikate valimi, mille parameetrid on definitsiooni kohaselt täpselt teada. Nende mudelparameetrite põhjal koostasime galaktikate pildid, millele lisasime vaatlusliku müra. Seejärel koostasime saadud piltide põhjal fotomeetrilise mudeli, millest tulenesid tähelise ketta taastatud parameetrid. Vastavalt sellele, kas algsed ja uuesti modelleeritud parameetrid erinesid jõudsime järeldusele, et üldine heledusjaotus on hästi taastatav, kuid mõningasi probleeme esineb kõdunud parameetrite määramisel. Problemaatilisim on kõdumine galaktika kaldenurga ja ketta paksuse vahel, mis võib anda märkimisväärse määramatuse dünaamilise mudeli tulemustesse.

Et testida gaasi dünaamika mudeli rakendatavust ning uurida galaktikate gaasiketaste evolutsiooni, rakendasime saadud mudelit galaktikatele, mis asuvad kaugustel kuni punanihe ~ 1. Valimis olevad galaktikad paistavad taevas väga väikesed, suuruselt võrreldavad spektrograafi pilu ning atmosfääri turbulentside tõttu kujutise moonutuste suurusega. Eelnimetatud efektid tekitavad märkimisväärse mõjutuse mõõdetud galaktika pöörlemiskõveratele, mistõttu dünaamilise modelleerimise põhjal leitud gaasiketta parameetrid ei ole täpsed, kuid statistiliselt võivad nad anda pädeva hinnangu gaasiketta suurustele. Stellaardünaamika mudeli rakendamise näiteks valisime lähedase galaktika M31, kuna see on põhjalikult uuritud galaktika, mille kohta on head ja mitmekesised vaatlused olemas. Rakendamise raskus seisnes Jeansi võrrandite kooskõlla viimisel kolmanda integraali teooriaga. Seda sai tehtud komponentide kaupa: mõhna kooskõla oli suurepärane, ketta oma rahuldav. Dünaamilise mudeli rakendamine näitas, et tuletatud meetod on toimiv ja perspektiivikas.

Antud töö käigus sai uuritud üht vähearvestatud, kuid potentsiaalselt märkimisväärset efekti – tolmu paiknemise mõju kinemaatilistele suurustele uuritavas galaktikas. Me näitasime, et see efekt on märkimisväärne suure kaldenurgaga galaktikate korral ning erinevus võib olla kuni mõnikümmend protsenti kiiruste dispersiooni korral ja kuni kümmekond protsenti pöörlemiskiiruste korral. Tolmu tõttu neeldumine on oluline arvesse võtta suure kaldenurgaga galaktikates, kus ta annab märkimisväärse mõju kinemaatilistele suurustele ning seega ka modelleeritud massi jaotusele.

Kokkuvõtvalt võib öelda, et antud doktoritöö tulemusena lisasime ühe meetodi dünaamiliste modelleerimise meetodite perekonda, mis võimaldab, võrreldes teiste meetoditega, arvesse võtta Kuzmini kolmanda integraali teooriast tulenevaid seoseid. Lisaks võimaldavad taolised dünaamilised mudelid arvesse võtta infot kogu galaktika ulatuses, mis osutub äärmiselt kasulikuks integraalvälja spektroskoopiliste vaatluste modelleerimise korral. Viimased vaatlused on hoogustunud ning tööpõld ees on lai.

BIBLIOGRAPHY

Afanasiev, V. L. & Popović, L. Č. 2015, *Polarization in linesa new method for measuring black hole masses in active galaxies*, ApJ, 800, L35

An, J. H. & Evans, N. W. 2009, *A theorem on central velocity dispersions*, ApJ, 701, 1500

Baes, M., Davies, J. I., Dejonghe, H., et al. 2003, *Radiative transfer in disc galaxies - III. The observed kinematics of dusty disc galaxies*, MNRAS, 343, 1081

Baes, M. & Dejonghe, H. 2000, *Kinematics of elliptical galaxies with a diffuse dust component*, MNRAS, 313, 153

Baes, M. & van Hese, E. 2007, *Dynamical models with a general anisotropy profile*, A&A, 471, 419

Bender, R. 1990, *Unraveling the kinematics of early-type galaxies - Presentation of a new method and its application to NGC4621*, A&A, 229, 441

Berta, S., Magnelli, B., Nordon, R., et al. 2011, *Building the cosmic infrared background brick by brick with Herschel/PEP*, A&A, 532, A49

Bianchi, S. 2007, *The dust distribution in edge-on galaxies. Radiative transfer fits of V and K'-band images*, A&A, 471, 765

Bianchini, P., Norris, M. A., van de Ven, G., et al. 2016, *The Effect of Unresolved Binaries on Globular Cluster Proper-motion Dispersion Profiles*, The Astrophysical Journal Letters, 820, L22

Binney, J. & Mamon, G. A. 1982, *M/L and velocity anisotropy from observations of spherical galaxies, or must M87 have a massive black hole*, MNRAS, 200, 361

Binney, J. & McMillan, P. J. 2016, *Torus mapper: a code for dynamical models of galaxies*, MNRAS, 456, 1982

Binney, J. & Tremaine, S. 2008, GalacticdDynamics: second edition (Princeton University Press)

Binney, J. J., Davies, R. L., & Illingworth, G. D. 1990, *Velocity mapping and models of the elliptical galaxies NGC 720, NGC 1052, and NGC 4697*, ApJ, 361, 78

Bottema, R. 1993, *The stellar kinematics of galactic disks*, A&A, 275, 16

Bovy, J. & Tremaine, S. 2012, *On the local dark matter density*, ApJ, 756, 89

Büdenbender, A., van de Ven, G., & Watkins, L. L. 2015, *The tilt of the velocity ellipsoid in the Milky Way disc*, MNRAS, 452, 956

Bundy, K., Bershady, M. A., Law, D. R., et al. 2015, *Overview of the SDSS-IV MaNGA survey: mapping nearby galaxies at Apache Point Observatory*, ApJ, 798, 7

Calzetti, D. 1999, *UV emission and bust properties of high redshift galaxies*, Ap&SS, 266, 243

Candlish, G. N., Smith, R., Moni Bidin, C., & Gibson, B. K. 2016, *Weighing the galactic disc using the Jeans equation: lessons from simulations*, MNRAS, 456, 3456

Cappellari, M. 2008, *Measuring the inclination and mass-to-light ratio of axisymmetric galaxies via anisotropic Jeans models of stellar kinematics*, MNRAS, 390, 71

Cappellari, M., Bacon, R., Bureau, M., et al. 2006, *The SAURON project - IV. The mass-to-light ratio, the virial mass estimator and the Fundamental Plane of elliptical and lenticular galaxies*, MNRAS, 366, 1126

Cappellari, M. & Emsellem, E. 2004, *Parametric recovery of line-of-sight velocity distributions from absorption-line spectra of galaxies via penalized likelihood*, PASP, 116, 138

Cappellari, M., Emsellem, E., Bacon, R., et al. 2007, *The SAURON project - X. The orbital anisotropy of elliptical and lenticular galaxies: revisiting the (V/σ, ϵ) diagram with integral-field stellar kinematics*, MNRAS, 379, 418

Cappellari, M., Romanowsky, A. J., Brodie, J. P., et al. 2015, *Small scatter and nearly isothermal mass profiles to four half-light eadii from two-dimensional stellar dynamics of early-type galaxies*, ApJ, 804, L21

Cappellari, M., Verolme, E. K., van der Marel, R. P., et al. 2002, *The counterrotating core and the black hole mass of IC 1459*, ApJ, 578, 787

Carollo, C. M., de Zeeuw, P. T., & van der Marel, R. P. 1995, *Velocity profiles of Osipkov-Merritt models*, MNRAS, 276, 1131

Chemin, L., Carignan, C., & Foster, T. 2009, *H I kinematics and dynamics of Messier 31*, ApJ, 705, 1395

Cinzano, P., Rix, H.-W., Sarzi, M., et al. 1999, *The kinematics and the origin of the ionized gas in NGC 4036*, MNRAS, 307, 433

Cinzano, P. & van der Marel, R. P. 1994, *Observations and dynamical modelling of the e4 galaxy NGC2974 - evidence for an embedded stellar disc*, MNRAS, 270, 325

Ciotti, L. 1996, *The analytical distribution function of anisotropic two-component Hernquist models*, ApJ, 471, 68

Ciotti, L., Lanzoni, B., & Renzini, A. 1996, *The tilt of the fundamental plane of elliptical galaxies - I. Exploring dynamical and structural effects*, MNRAS, 282, 1

Ciotti, L., Morganti, L., & de Zeeuw, P. T. 2009, *Two-component galaxies with flat rotation curve*, MNRAS, 393, 491

Corbelli, E., Lorenzoni, S., Walterbos, R., Braun, R., & Thilker, D. 2010, *A wide-field H I mosaic of Messier 31. II. The disk warp, rotation, and the dark matter halo*, A&A, 511, A89

Corsini, E. M., Bertola, F., Sarzi, M., et al. 1999, *The kinematics and the origin of the ionized gas in NGC 4036*, in The formation of galactic bulges, ed. C. M. Carollo, H. C. Ferguson, & R. F. G. Wyse, 170

Cretton, N., de Zeeuw, P. T., van der Marel, R. P., & Rix, H.-W. 1999, *Axisymmetric three-integral models for galaxies*, ApJS, 124, 383

Cretton, N. & van den Bosch, F. C. 1999, *Evidence for a massive black hole in the S0 galaxy NGC 4342*, ApJ, 514, 704

da Cunha, E., Charlot, S., & Elbaz, D. 2008, *A simple model to interpret the ultraviolet, optical and infrared emission from galaxies*, MNRAS, 388, 1595

Davies, R. L., Efstathiou, G., Fall, S. M., Illingworth, G., & Schechter, P. L. 1983, *The kinematic properties of faint elliptical galaxies*, ApJ, 266, 41

Dehnen, W. 1993, *A family of potential-density pairs for spherical galaxies and bulges*, MNRAS, 265, 250

Dehnen, W. 1998, *The distribution of nearby stars in velocity space inferred from HIPPARCOS data*, AJ, 115, 2384

Dehnen, W. & Binney, J. J. 1998, *Local stellar kinematics from HIPPARCOS data*, MNRAS, 298, 387

Dehnen, W. & McLaughlin, D. E. 2005, *Dynamical insight into dark matter haloes*, MNRAS, 363, 1057

Dehnen, W., McLaughlin, D. E., & Sachania, J. 2006, *The velocity dispersion and mass profile of the Milky Way*, MNRAS, 369, 1688

Devereux, N., Ford, H., Tsvetanov, Z., & Jacoby, G. 2003, *STIS spectroscopy of the central 10 parsecs of M81: evidence for a massive black hole*, AJ, 125, 1226

Dhar, B. K. & Williams, L. L. R. 2010, *Surface mass density of the Einasto family of dark matter haloes: are they Sersic-like?*, MNRAS, 405, 340

Drehmer, D. A., Storchi-Bergmann, T., Ferrari, F., Cappellari, M., & Riffel, R. A. 2015, *The benchmark black hole in NGC 4258: dynamical models from high-resolution two-dimensional stellar kinematics*, MNRAS, 450, 128

Einasto, J. 1969, *The andromeda galaxy M 31: I. A preliminary model*, Astrophysics, 5, 67

Einasto, J. 1970, *The Andromeda galaxy M31. II. Hydrodynamical model. Theory*, Astrophysics, 6, 69

Einasto, J., Kaasik, A., & Saar, E. 1974, *Dynamic evidence on massive coronas of galaxies*, Nature, 250, 309

Emsellem, E., Monnet, G., & Bacon, R. 1994, *The multi-gaussian expansion method: a tool for building realistic photometric and kinematical models of stellar systems I. The formalism*, A&A, 285, 723

ESA, ed. 1997, ESA Special Publication, Vol. 1200, The HIPPARCOS and TYCHO catalogues. Astrometric and photometric star catalogues derived from the ESA HIPPARCOS Space Astrometry Mission

Falco, M., Mamon, G. A., Wojtak, R., Hansen, S. H., & Gottlöber, S. 2013, *Dynamical signatures of infall around galaxy clusters: a generalized Jeans equation*, MNRAS, 436, 2639

Feroz, F. & Hobson, M. P. 2008, *Multimodal nested sampling: an efficient and robust alternative to Markov Chain Monte Carlo methods for astronomical data analyses*, MNRAS, 384, 449

Feroz, F., Hobson, M. P., & Bridges, M. 2009, *MULTINEST: an efficient and robust Bayesian inference tool for cosmology and particle physics*, MNRAS, 398, 1601

Feroz, F., Hobson, M. P., Cameron, E., & Pettitt, A. N. 2013, *Importance nested sampling and the MultiNest algorithm*, arXiv:1306.2144

Fujimoto, Y., Tasker, E. J., & Habe, A. 2014, *Environmental dependence of star formation induced by cloud collisions in a barred galaxy*, MNRAS, 445, L65

Garrido Pestaña, J. L. & Eckhardt, D. H. 2010, *The futile search for Galactic disk dark matter*, ApJ, 722, L70

Geehan, J. J., Fardal, M. A., Babul, A., & Guhathakurta, P. 2006, *Investigating the Andromeda stream - I. Simple analytic bulge-disc-halo model for M31*, MNRAS, 366, 996

Gerssen, J., Kuijken, K., & Merrifield, M. R. 1997, *The shape of the velocity ellipsoid in NGC 488*, MNRAS, 288, 618

Giavalisco, M., Ferguson, H. C., Koekemoer, A. M., et al. 2004, *The Great Observatories Origins Deep Survey: initial results from optical and near-infrared imaging*, ApJ, 600, L93

Gnerucci, A., Marconi, A., Capetti, A., et al. 2011, *Spectroastrometry of rotating gas disks for the detection of supermassive black holes in galactic nuclei. II. Application to the galaxy Centaurus A (NGC 5128)*, A&A, 536, A86

Grand, R. J. J., Springel, V., Gómez, F. A., et al. 2016, *Vertical disc heating in Milky Way-sized galaxies in a cosmological context*, MNRAS

Grazian, A., Fontana, A., de Santis, C., et al. 2006, *The GOODS-MUSIC sample: a multicolour catalog of near-IR selected galaxies in the GOODS-South field*, A&A, 449, 951

Halliday, C., Carter, D., Bridges, T. J., et al. 2006, *Planetary nebula velocities in the disc and bulge of M31*, MNRAS, 369, 97

Hernquist, L. 1990, *An analytical model for spherical galaxies and bulges*, ApJ, 356, 359

Hjorth, J. 1994, *Stability against phase mixing of collisionless self-gravitating matter*, ApJ, 424, 106

Holmberg, J. & Flynn, C. 2004, *The local surface density of disc matter mapped by Hipparcos*, MNRAS, 352, 440

Howell, S. B. 2006, Handbook of CCD Astronomy, ed. R. Ellis, J. Huchra, S. Kahn, G. Rieke, & P. B. Stetson

Hunter, D. R. 2014, *Derivation of the anisotropy profile, constraints on the local velocity dispersion, and implications for direct detection*, , 2, 23

Ida, S., Kokubo, E., & Makino, J. 1993, *The origin of anisotropic velocity dispersion of particles in a disc potential*, MNRAS, 263, 875

Jaffe, W. 1983, *A simple model for the distribution of light in spherical galaxies*, MNRAS, 202, 995

Jalali, M. A. & Tremaine, S. 2011, *Generalized Schwarzschild's method*, MNRAS, 410, 2003

Jeans, J. H. 1915, *On the theory of star-streaming and the structure of the universe*, MNRAS, 76, 70

Joseph, C. L., Merritt, D., Olling, R., et al. 2001, *The nuclear dynamics of M32. I. Data and stellar kinematics*, ApJ, 550, 668

Kormendy, J. 1988, *Evidence for a supermassive black hole in the nucleus of M31*, ApJ, 325, 128

Kormendy, J. & Bender, R. 1999, *The double nucleus and central black hole of M31*, ApJ, 522, 772

Kuzmin, G. 1953, *The third integral of stellar motion and the dynamics of the stationary Galaxy (in Russian)*, Publication of Tartu Astron. Obervatory, 32, 332

Kuzmin, G. 1956, *Model of the steady galaxy allowing of the triaxial distribution of velocities (in Russian)*, Publication of Tartu Astron. Obervatory, 33, 27

Kuzmin, G. G. 1961, *On the variation of the dispersion of stellar velocities (in Russian)*, Publication of Tartu Astron. Obervatory, 33, 351

Lanzoni, B. & Ciotti, L. 2003, *Projection effects on the FP thickness. A Monte-Carlo exploration*, A&A, 404, 819

Leroy, A. K., Bolatto, A., Gordon, K., et al. 2011, *The CO-to-H_2 conversion factor from infrared dust emission across the Local Group*, ApJ, 737, 12

Lindblad, B. 1934, *On the constitution and development of rotating stellar systems*, MNRAS, 95, 12

Łokas, E. L. 2002, *Dark matter distribution in dwarf spheroidal galaxies*, MNRAS, 333, 697

Łokas, E. L. & Mamon, G. A. 2001, *Properties of spherical galaxies and clusters*

with an NFW density profile, MNRAS, 321, 155

Magorrian, J., Tremaine, S., Richstone, D., et al. 1998, *The demography of massive dark objects in galaxy centers*, AJ, 115, 2285

Malvido, J. C. & Sellwood, J. A. 2015, *Made-to-measure models of self-similar triaxial haloes with steep inner density gradients*, MNRAS, 449, 2553

McElroy, D. B. 1983, *Dynamics of the stellar component of the bulge of M31*, ApJ, 270, 485

Merrett, H. R., Merrifield, M. R., Douglas, N. G., et al. 2006, *A deep kinematic survey of planetary nebulae in the Andromeda galaxy using the Planetary Nebula Spectrograph*, MNRAS, 369, 120

Merrifield, M. R. & Kent, S. M. 1990, *Fourth moments and the dynamics of spherical systems*, AJ, 99, 1548

Meza, A. & Zamorano, N. 1997, *Numerical stability of a family of Osipkov-Merritt models*, ApJ, 490, 136

Minchev, I. & Quillen, A. C. 2006, *Radial heating of a galactic disc by multiple spiral density waves*, MNRAS, 368, 623

Minchev, I. & Quillen, A. C. 2007, *The effect of spiral structure on the measurements of the Oort constants*, MNRAS, 377, 1163

Mogotsi, K. M., de Blok, W. J. G., Caldú-Primo, A., et al. 2016, *Hi and CO velocity dispersions in nearby galaxies*, AJ, 151, 15

Molaeinezhad, A., Falcón-Barroso, J., Martínez-Valpuesta, I., et al. 2016, *Establishing the level of cylindrical rotation in boxy/peanut bulges*, MNRAS, 456, 692

Moni Bidin, C., Carraro, G., Méndez, R. A., & Smith, R. 2012, *Kinematical and chemical vertical structure of the Galactic thick disk. II. A lack of dark matter in the Solar neighborhood*, ApJ, 751, 30

Navarro, J. F., Hayashi, E., Power, C., et al. 2004, *The inner structure of ΛCDM haloes - III. Universality and asymptotic slopes*, MNRAS, 349, 1039

Nowak, N., Saglia, R. P., Thomas, J., et al. 2007, *The supermassive black hole in NGC4486a detected with SINFONI at the Very Large Telescope*, MNRAS, 379, 909

Onken, C. A., Valluri, M., Brown, J. S., et al. 2014, *The black hole mass of NGC 4151. II. Stellar dynamical measurement from near-infrared integral field spectroscopy*, ApJ, 791, 37

Perryman, M. A. C., de Boer, K. S., Gilmore, G., et al. 2001, *GAIA: composition, formation and evolution of the Galaxy*, A&A, 369, 339

Press, W. H., Teukolsky, S. A., Vetterling, W. T., & Flannery, B. P. 1992, Numerical recipes in FORTRAN. The art of scientific computing

Riciputi, A., Lanzoni, B., Bonoli, S., & Ciotti, L. 2005, *The contribution of rotational velocity to the FP of elliptical galaxies*, A&A, 443, 133

Rix, H.-W. & White, S. D. M. 1992, *Optimal estimates of line-of-sight velocity distributions from absorption line spectra of galaxies - Nuclear discs in elliptical galaxies*, MNRAS, 254, 389

Rubin, V. C. & Ford, Jr., W. K. 1970, *Rotation of the Andromeda Nebula from a spectroscopic survey of emission regions*, ApJ, 159, 379

Rubin, V. C., Ford, W. K. J., & . Thonnard, N. 1980, *Rotational properties of 21 SC galaxies with a large range of luminosities and radii, from NGC 4605 /R = 4kpc/ to UGC 2885 /R = 122 kpc/*, ApJ, 238, 471

Saglia, R. P., Fabricius, M., Bender, R., et al. 2010, *The old and heavy bulge of M 31 . I. Kinematics and stellar populations*, A&A, 509, A61

Sánchez, S. F., Kennicutt, R. C., Gil de Paz, A., et al. 2012, *CALIFA, the Calar Alto Legacy Integral Field Area survey. I. survey presentation*, A&A, 538, A8

Sánchez-Salcedo, F. J., Flynn, C., & de Diego, J. A. 2016, *Jeans analysis of the Galactic thick disk and the local dark matter density*, ApJ, 817, 13

Sánchez-Salcedo, F. J., Flynn, C., & Hidalgo-Gámez, A. M. 2011, *On the vertical equilibrium of the local Galactic disk and the search for disk dark matter*, ApJ, 731, L35

Sarzi, M., Falcón-Barroso, J., Davies, R. L., et al. 2006, *The SAURON project - V. Integral-field emission-line kinematics of 48 elliptical and lenticular galaxies*, MNRAS, 366, 1151

Satoh, C. 1980, *Dynamical models of axisymmetric galaxies and their applications to the elliptical galaxy NGC4697*, PASJ, 32, 41

Saxton, C. J. & Ferreras, I. 2010, *Polytropic dark haloes of elliptical galaxies*, MNRAS, 405, 77

Schlegel, D. J., Finkbeiner, D. P., & Davis, M. 1998, *Maps of dust infrared emission for use in estimation of reddening and cosmic microwave background radiation foregrounds*, ApJ, 500, 525

Schmidt, K. B., Hansen, S. H., An, J. H., Williams, L. L. R., & Macciò, A. V. 2009, *Dark matter angular momentum profile from the Jeans equation*, ApJ, 694, 893

Schwarzschild, M. 1979, *A numerical model for a triaxial stellar system in dynamical equilibrium*, ApJ, 232, 236

Seigar, M. S., Barth, A. J., & Bullock, J. S. 2008, *A revised Λ CDM mass model for the Andromeda Galaxy*, MNRAS, 389, 1911

Sellwood, J. A. 2013, *Relaxation in N-body simulations of disk galaxies*, ApJ, 769, L24

Sersic, J. L. 1968, Atlas de galaxias australes

Smet, C. O., Posacki, S., & Ciotti, L. 2015, *Miyamoto-Nagai discs embedded in the Binney logarithmic potential: analytical solution of the two-integrals Jeans equations*, MNRAS, 448, 2921

Smith, M. C., Whiteoak, S. H., & Evans, N. W. 2012, *Slicing and dicing the Milky Way disk in the Sloan Digital Sky Survey*, ApJ, 746, 181

Sparre, M. & Hansen, S. H. 2012, *Asymmetric velocity anisotropies in remnants of collisionless mergers*, , 7, 42

Statler, T. S., Dejonghe, H., & Smecker-Hane, T. 1999, *The three-dimensional mass distribution in NGC 1700*, AJ, 117, 126

Statler, T. S., Emsellem, E., Peletier, R. F., & Bacon, R. 2004, *Long-lived triaxiality in the dynamically old elliptical galaxy NGC 4365: a limit on chaos and black hole mass*, MNRAS, 353, 1

Takeuchi, T. M., Ohta, K., Yuma, S., & Yabe, K. 2015, *When did round disk galaxies form?*, ApJ, 801, 2

Tamm, A., Tempel, E., Tenjes, P., Tihhonova, O., & Tuvikene, T. 2012, *Stellar mass map and dark matter distribution in M 31*, A&A, 546, A4

Tamm, A. & Tenjes, P. 2006, *Surface photometry and structure of high redshift disk galaxies in the HDF-S NICMOS field*, A&A, 449, 67

Tempel, E., Tamm, A., & Tenjes, P. 2007, *Visible and dark matter in M 31 - II. A dynamical model and dark matter density distribution*, arXiv:0707.4374

Tempel, E. & Tenjes, P. 2006, *Line-of-sight velocity dispersions and a mass-distribution model of the Sa galaxy NGC 4594*, MNRAS, 371, 1269

Tenjes, P., Einasto, J., Maitzen, H. M., & Zinnecker, H. 2001, *Origin and possible birthplace of the extreme runaway star HIP 60350*, A&A, 369, 530

Tremaine, S., Richstone, D. O., Byun, Y.-I., et al. 1994, *A family of models for spherical stellar systems*, AJ, 107, 634

Valluri, M., Merritt, D., & Emsellem, E. 2004, *Difficulties with recovering the masses of supermassive black holes from stellar kinematical data*, ApJ, 602, 66

van Albada, T. S., Bertin, G., & Stiavelli, M. 1995, *Estimating distances to elliptical galaxies with a mass-luminosity relation*, MNRAS, 276, 1255

van de Ven, G., de Zeeuw, P. T., & van den Bosch, R. C. E. 2008, *Recovery of the internal orbital structure of galaxies*, MNRAS, 385, 614

van der Kruit, P. C. & de Grijs, R. 1999, *On the axis ratio of the stellar velocity ellipsoid in disks of spiral galaxies*, A&A, 352, 129

van der Marel, R. P., Cretton, N., de Zeeuw, P. T., & Rix, H.-W. 1998, *Improved evidence for a black hole in M32 from HST/FOS spectra. II. Axisymmetric dynamical models*, ApJ, 493, 613

van der Marel, R. P., Rix, H. W., Carter, D., et al. 1994, *Velocity profiles of galaxies with claimed black-holes - part one - observations of M31 M32 NGC3115 and NGC4594*, MNRAS, 268, 521

Van Hese, E., Baes, M., & Dejonghe, H. 2009, *The dynamical structure of dark matter halos with universal properties*, ApJ, 690, 1280

Vasiliev, E. & Athanassoula, E. 2015, *Applying Schwarzschild's orbit superposition method to barred or non-barred disc galaxies*, MNRAS, 450, 2842

Vera-Ciro, C. A., Sales, L. V., Helmi, A., & Navarro, J. F. 2014, *The shape of dark matter subhaloes in the Aquarius simulations*, MNRAS, 439, 2863

Viaene, S., De Geyter, G., Baes, M., et al. 2015, *NGC 4370: a case study for testing our ability to infer dust distribution and mass in nearby galaxies*, A&A, 579, A103

Vorobyov, E. I. & Theis, C. 2008, *Shape and orientation of stellar velocity ellipsoids in spiral galaxies*, MNRAS, 383, 817

Vulcani, B., Bamford, S. P., Häußler, B., et al. 2014, *Galaxy And Mass Assembly (GAMA): the wavelength-dependent sizes and profiles of galaxies revealed by MegaMorph*, MNRAS, 441, 1340

Walter, F., Brinks, E., de Blok, W. J. G., et al. 2008, *THINGS: The H I Nearby Galaxy Survey*, AJ, 136, 2563

Weiner, B. J., Willmer, C. N. A., Faber, S. M., et al. 2006, *A survey of galaxy kinematics to z˜1 in the TKRS/GOODS-N Field. I. Rotation and dispersion properties*, ApJ, 653, 1027

Wirth, G. D., Trump, J. R., Barro, G., et al. 2015, *The Team Keck Redshift Survey 2: MOSFIRE spectroscopy of the GOODS-North field*, AJ, 150, 153

Wirth, G. D., Willmer, C. N. A., Amico, P., et al. 2004, *The Team Keck Treasury Redshift Survey of the GOODS-North field*, AJ, 127, 3121

Xilouris, E. M., Byun, Y. I., Kylafis, N. D., Paleologou, E. V., & Papamastorakis, J. 1999, *Are spiral galaxies optically thin or thick?*, A&A, 344, 868

York, D. G., Adelman, J., Anderson, Jr., J. E., et al. 2000, *The Sloan Digital Sky Survey: technical summary*, AJ, 120, 1579

Young, L. M., Bureau, M., & Cappellari, M. 2008, *Structure and kinematics of molecular disks in fast-rotator early-type galaxies*, ApJ, 676, 317

Yurin, D. & Springel, V. 2014, *An iterative method for the construction of N-body galaxy models in collisionless equilibrium*, MNRAS, 444, 62

Zait, A., Hoffman, Y., & Shlosman, I. 2008, *Dark matter halos: velocity anisotropy-density slope relation*, ApJ, 682, 835

Zhao, Y., Peng, Q., & Hu, T. 2006, *A new method to determine the thickness of non-edge-on disk galaxies*, A&A, 452, 451

Zou, H., Yang, Y.-B., Zhang, T.-M., et al. 2011, *Kinematics and stellar population properties of the Andromeda galaxy by using the spectroscopic observations of the Guoshoujing Telescope*, Research in Astronomy and Astrophysics, 11, 1093

ACKNOWLEDGEMENTS

I am very grateful to my supervisors Dr. Elmo Tempel and Prof. Peeter Tenjes for their patient supervision and teaching. Elmo has taught me how science works and a great amount of useful traits. Peeter provided me insights into his deep understanding of galaxy dynamics and physics. I am also very thankful for their advice on improving my manuscript.

My sincere gratitude goes to my colleagues at Tartu Observatory Antti Tamm and Olga Tihhonova for the fruitful collaboration and their contribution to the studies.

I would like to thank Radu Stoica for his support and hospitality during my stay at the Lille University in France. This visit gave me vital support to my research and allowed me to finalise my thesis.

I acknowledge the financial support by the Estonian Science Foundation and the Estonian Ministry of Education and the European Regional Development Fund (TK133).

PUBLICATIONS

CURRICULUM VITAE

Personal data

Name	Rain Kipper
Date and place of birth	6 March 1988, Viljandi, Estonia
Citizenship	Estonian
Current employment	Tartu Observatory
Address	Tartu Observatory 61602 Tõravere Tartumaa, Estonia
Phone	(+372) 58 528 417
E-mail	rain.kipper@to.ee

Education

1995 – 2007	Viljandi Country Gymnasium
2007 – 2010	University of Tartu, undergraduate student, BSc 2010 (physics)
2010 – 2012	University of Tartu, graduate student, MSc 2012 (physics)
2012 – 2016	University of Tartu, PhD student

Employment

2010 – 2012	Tartu Observatory, Engineer
2012 – 2016	Tartu Observatory, Junior Researcher

Professional training

16.07 – 27.07 2012	Summer school “Summer School on Cosmology”, Trieste, Italy.
07.01 – 18.01 2013	Winter school “Nordita Winter School 2013 in High-Energy Astrophysics”, Stockholm, Sweden.
30.06 – 09.07 2014	Summer school “CSC Summer School in High-performance computing”, Nuuksio, Finland.

24.08 – 28.08 2014	Summer school “Scientific Writing for Young Astronomers”, Tihany, Hungary.
15.07 – 25.07 2015	Summer school “Introduction to Cosmology”, Kielce, Poland.
01.06 – 06.06 2015	Summer school “Summer School in Statistics for Astronomers XI”, Pennsylvania, USA.

Conference presentations

21.09 – 22.09 2011	Conference “Tartu - Tuorla annual meeting 2011: Remote sensing of the Universe” Tartu, Estonia. *Oral presentation*: “Kinematics of distant galaxies”
06.05 – 09.05 2012	Conference “Baltic Applied Astroinformatics and Space data Processing”, Venspils, Latvia. *Oral presentation*: “Kinematics of distant galaxies”
23.06 – 28.06 2014	Conference “IAU 308: The Zeldovich Universe”, Tallinn, Estonia. *Poster presentation*: “The properties of gaseous discs”
23.06 – 28.06 2014	Conference “IAU 308: The Zeldovich Universe”, Tallinn, Estonia. *Poster presentation*: “Fundamental plane of SDSS galaxies as function of environment”
01.10 – 04.10 2014	Conference “Tartu – Tuorla annual meeting 2014. Small and Large scale Universe”, Tuorla, Estonia. *Oral presentation*: “Fundamental plane of galaxies”
22.09 – 25.09 2015	Conference “Tartu – Tuorla annual meeting 2015. (Always Look on) The Bright Side of Space”, Kubija, Estonia. *Oral presentation*: “Dynamical side on Andromeda galaxy”

Language skills

Estonian	the first language
English	good

Honours and Awards

2012	E. Öpik stipend (Tartu Observatory)

Fields of research

Photometrical and dynamical modelling of galaxies.
Galaxy groups and filaments in the cosmic web.

Publications

R. Kipper, E. Tempel, and A. Tamm. Kinematic Modeling of Distant Galaxies. *Baltic Astronomy*, 21,523–529, 2012.

E. Tempel, R. Kipper, E. Saar, M. Bussov, A. Hektor, and J. Pelt. Galaxy filaments as pearl necklaces. A&A, 572,A8, December 2014a.

E. Tempel, A. Tamm, M. Gramann, T. Tuvikene, L. J. Liivamägi, I. Suhhonenko, R. Kipper, M. Einasto, and E. Saar. Flux- and volume-limited groups/clusters for the SDSS galaxies: catalogues and mass estimation. A&A, 566,A1, June 2014b.

E. Tempel, Q. Guo, R. Kipper, and N. I. Libeskind. The alignment of satellite galaxies and cosmic filaments: observations and simulations. MNRAS, 450, 2727–2738, July 2015.

E. Tempel, A. Tamm, R. Kipper, and P. Tenjes. Recovering 3D structural properties of galaxies from SDSS-like photometry. *Research in Astronomy and Astrophysics*, 15,1613, Oct 2015.

E. Tempel, R. Kipper, A. Tamm, M. Gramann, M. Einasto, T. Sepp, and T. Tuvikene. Friends-of-friends galaxy group finder with membership refinement. Application to the local Universe. A&A, 572,A8, Apr 2016.

E. Tempel, R. Stoica, R. Kipper and E. Saar. Bisous model-Detecting filamentary patterns in point processes. *Astronomy and Computing*, 16,17, Jul 2016.

R. Kipper, P. Tenjes, A. Tamm, O. Tihhonova and E. Tempel. Stellar kinematics using a third integral of motion: method and application on the Andromeda galaxy. MNRAS, accepted for publication. May 2016.

ELULOOKIRJELDUS

Isikuandmed

Nimi	Rain Kipper
Sünniaeg ja -koht	6. märts 1988, Viljandi, Eesti
Kodakondsus	eesti
Praegune töökoht	Tartu Observatoorium
Aadress	Observatoorium 1, 61602 Tõravere Tartumaa, Eesti
Telefon	(+372) 58 528 417
E-post	rain.kipper@to.ee

Haridustee

1995 – 2007	Viljandi Maagümnaasium
2007 – 2010	Tartu Ülikool, üliõpilane, BSc 2010 (füüsika)
2010 – 2012	Tartu Ülikool, magistrant, MSc 2012 (füüsika)
2012 – 2016	Tartu Ülikool, doktorant

Teenistuskäik

2010 – 2012	Tartu Observatoorium, insener
2012 – . . .	Tartu Observatoorium, nooremteadur

Täiendkoolitus

16.07 – 27.07 2012	Suvekool “Summer School on Cosmology”, Trieste, Itaalia.
07.01 – 18.01 2013	Talvekool “Nordita Winter School 2013 in High–Energy Astrophysics”, Stockholm, Rootsi.
30.06 – 09.07 2014	Suvekool “CSC Summer School in High-performance computing”, Nuuksio, Soome.
24.08 – 28.08 2014	Suvekool “Scientific Writing for Young Astronomers”, Tihany, Ungari.

15.07 – 25.07 2015	Suvekool “Introduction to Cosmology”, Kielce, Poola.
01.06 – 06.06 2015	Suvekool “Summer School in Statistics for Astronomers XI”, Pennsylvania, USA.

Konverentside ettekanded

21.09 – 22.09 2011	Konverents “Tartu - Tuorla annual meeting 2011: Remote sensing of the Universe”, Tartu, Eesti. *Suuline ettekanne*: “Kinematics of distant galaxies”
06.05 – 09.05 2012	Konverents “Baltic Applied Astroinformatics and Space data Processing”, Venspils, Läti. *Suuline ettekanne*: “Kinematics of distant galaxies”
23.06 – 28.06 2014	Konverents “IAU 308: The Zeldovich Universe”, Tallinn, Eesti. *Poster*: “The properties of gaseous discs”
23.06 – 28.06 2014	Konverents “IAU 308: The Zeldovich Universe”, Tallinn, Eesti. *Poster*: “Fundamental plane of SDSS galaxies as function of environment”
01.10 – 04.10 2014	Konverents “Tartu – Tuorla annual meeting 2014. Small and Large scale Universe”, Turola, Soome. *Suuline ettekanne*: “Fundamental plane”
22.09 – 25.09 2015	Konverents “Tartu – Tuorla annual meeting 2015. (Always Look on) The Bright Side of Space”, Kubija, Eesti. *Suuline ettekanne*: “Dynamical side on Andromeda galaxy”

Keelteoskus

eesti keel	emakeel
inglise keel	hea

Uurimistoetused ja stipendiumid

2012	E. Öpik stipendium (Tartu Observatoorium)

Peamised uurimissuunad

Galaktikate fotomeetriline ja dünaamiline modelleerimine.
Galaktikate grupid ja filamendid.

DISSERTATIONES ASTRONOMIAE UNIVERSITATIS TARTUENSIS

1. **Tõnu Viik.** Numerical realizations of analytical methods in theory of radiative transfer. Tartu, 1991.
2. **Enn Saar.** Geometry of the large scale structure of the Universe. Tartu, 1991.
3. **Maret Einasto.** Morphological and luminosity segregation of galaxies. Tartu, 1991.
4. **Urmas Haud.** Dark Matter in galaxies. Tartu, 1991.
5. **Eugene A. Ustinov.** Inverse problems of radiative transfer in sounding of planetary atmospheres. Tartu, 1992.
6. **Peeter Tenjes.** Models of regular galaxies. Tartu, 1993.
7. **Ivar Suisalu.** Simulation of the evolution of large scale structure elements with adaptive multigrid method. Tartu, 1995.
8. **Teimuraz Shvelidze.** Automated quantitative spectral classification of stars by means of objective prism spectra: the method and applications. Tartu, 1999.
9. **Jelena Gerškevitš.** Formation and evolution of binary systems with compact objects. Tartu, 2002.
10. **Ivan Suhhonenko**. Large-scale motions in the universe. Tartu, 2003.
11. **Antti Tamm.** Structure of distant disk galaxies. Tartu, 2006.
12. **Vladislav-Veniamin Pustynski.** Modeling the reflection effect in pre-cataclysmic binary systems. Tartu, 2007.
13. **Anna Aret.** Evolutionary separation of mercury isotopes in atmospheres of chemically peculiar stars. Tartu, 2009.
14. **Mari Burmeister.** Characteristics of the hot components of symbiotic stars. Tartu, 2010.
15. **Elmo Tempel.** Tracing galaxy evolution by their present-day luminosity function. Tartu, 2011.
16. **Anti Hirv.** Estimation of time delays from light curves of gravitationally lensed quasars. Tartu, 2011.